Acta Pharmaceutica Sinica B 2026;16(3):1510−1529

Chinese Pharmaceutical Association
Institute of Materia Medica, Chinese Academy of Medical Sciences

Acta Pharmaceutica Sinica B

www.elsevier.com/locate/apsb
www.sciencedirect.com

ORIGINAL ARTICLE

Vitamin A and its analogues modulate MUFAs metabolism to improve ferroptosis and aging by direct targeting of ACSL3

Nanxuan Luo[a,†], Yijie Xiao[a,†], Yile Zhai[b,c,†], Jie Li[a], Lijie Lv[a], Houhua Yin[a], Fang Lin[a], Biwen Wan[a], Ke Zhang[a], Junchi Hu[a], Junyan Liu[a], Yongjun Dang[a], Yi He[a], Yahui Zhao[a], Zhe Zhang[b,c,*], Shenyou Nie[a,*], Hai-Xin Yuan[a,d,*]

[a]*Basic Medicine Research and Innovation Center for Novel Target and Therapeutic Intervention (Ministry of Education), Department of Cancer Center and Department of Urology of the Second Affiliated Hospital, College of Pharmacy, Chongqing Medical University, Chongqing 400016, China*
[b]*The Second Hospital, Cheeloo College of Medicine, Shandong University, Ji'nan 250033, China*
[c]*Department of Histology and Embryology, School of Basic Medical Sciences, Cheeloo College of Medicine, Shandong University, Ji'nan 250012, China*
[d]*The Fifth People's Hospital of Shanghai, Fudan University, Shanghai 200032, China*

Received 22 April 2025; received in revised form 6 August 2025; accepted 11 September 2025

KEY WORDS

Vitamin A;
All-*trans* retinoic acid;
Ferroptosis;
ACSL3;
Lipid metabolism;
Acute liver injury;
Aging;
Longevity

Abstract In our screening campaign for novel ferroptosis inhibitors, we identified that vitamin A (VA) and its metabolite all-*trans* retinoic acid (ATRA) exhibited potent ferroptosis-suppressing activity. Notably, through a combination of biochemical and pharmacological assays, we demonstrated that the anti-ferroptotic effects of VA and ATRA are independent of both antioxidative mechanisms and the canonical RAR/RXR signaling pathway. This conclusion was corroborated by a series of newly synthesized VA analogues. Furthermore, VA and its structural derivatives significantly alleviated ferroptosis-associated pathological phenotypes in murine models. Intriguingly, we discovered a novel function of VA and its analogues, which directly target acyl-CoA synthetase long-chain family member 3 (ACSL3) and enhance its enzymatic activity. This ACSL3-dependent mechanism increases the MUFA/PUFA ratio in phospholipids, thereby preventing lipid peroxidation. Strikingly, we further demonstrated that VA and its analogue D3 [(2*E*,4*E*,6*E*,8*E*)-*N*,3,7-trimethyl-9-(2,6,6-trimethylcyclohex-1-en-1-yl)nona-

*Corresponding authors.
E-mail addresses: zhezhang@sdu.edu.cn (Zhe Zhang), nieshenyou@cqmu.edu.cn (Shenyou Nie), yuanhaixin@cqmu.edu.cn (Hai-Xin Yuan).
[†]These authors made equal contributions to this work.
Peer review under the responsibility of Chinese Pharmaceutical Association and Institute of Materia Medica, Chinese Academy of Medical Sciences.

https://doi.org/10.1016/j.apsb.2025.11.004

2,4,6,8-tetraenamide] extend the lifespan of *C. elegans* in a manner dependent on ACSL3, highlighting the physiological relevance of this pathway in aging. Collectively, our findings unveil a previously unrecognized role for VA and its analogues in modulating lipid metabolism, thereby providing a theoretical basis for their potential application in treating ferroptosis-related diseases and possibly enhancing longevity.

1. Introduction

Ferroptosis is an iron-dependent form of non-apoptotic cell death characterized by extensive phospholipid peroxidation, resulting in plasma membrane damage and cell death[1]. Lipid peroxidation primarily targets esterified polyunsaturated fatty acids (PUFAs) rather than free PUFAs, with phospholipids (PLs) containing PUFA tails exhibiting heightened susceptibility to peroxidation at bis-allylic carbons[2]. Notably, phosphatidylethanolamines (PEs) and phosphatidylcholine (PCs) esterified with arachidonic acid (AA, C20:4) or arachidonic acid (AdA, C22:4) are more tightly associated with ferroptosis than other PLs[2,3]. Glutathione peroxidase 4 (GPX4) is the only mammalian enzyme identified to catalyze the conversion of phospholipid hydroperoxide into phospholipid alcohol, thus suppressing ferroptosis[4]. Moreover, there exist endogenous lipophilic radical trapping agents, including coenzyme Q10[5-7], vitamin E[2], tetrahydrobiopterin (BH_4)[8], vitamin K[9] and 7-dehydrocholesterol (7-DHC)[10,11], that inhibit ferroptosis by quenching lipid radicals.

The susceptibility of fatty acids to peroxidation hinges on their saturation status. Phospholipids with monoacyl-PUFA and diacyl-PUFA tails (*e.g.*, PC-$PUFA_2$) readily undergo peroxidation *via* labile iron or iron-containing enzymes, generating phospholipid hydroperoxides that propagate oxidative chain reactions within membranes[12,13]. A recent study reported that LPCAT1 preferentially incorporates saturated fatty acids (SFAs) into cellular membrane PLs while decreasing the levels of PL-PUFAs, resulting in increased resistance to ferroptosis[14]. Notably, monounsaturated fatty acids (MUFAs) have been recognized as a potent inhibitor of ferroptosis through competing with PUFAs for incorporation into PLs, a process that is dependent on ACSL3[15]. ACSL3 displays a marked preference for catalyzing the esterification of MUFAs with CoA, and the lyso-PL acyltransferases, specifically membrane bound *O*-acyltransferase domain containing 1 and 2 (MBOAT1/2)[16], selectively incorporate MUFA-CoA into PLs. This process results in an elevation of membrane PL-MUFAs and a concomitant reduction of PL-PUFAs, thereby serving as an intrinsic mechanism to combat ferroptosis. Another study reported that melanoma cells from lymph nodes evade ferroptosis by enriching phospholipids with oleic acid in a manner that is dependent on ACSL3[17]. Furthermore, the elevated expression of stearoyl-CoA desaturase (SCD1), an enzyme that catalyzes the biosynthesis of MUFAs from SFAs, confers ferroptosis resistance in ovarian cancer cells, mimicking the protective effects observed with MUFAs treatment[18]. Thus, genetic or pharmacological modulation of lipid metabolism and membrane PL remodeling may represent a potential therapeutic strategy for ferroptosis-associated diseases.

Numerous studies have indicated that ferroptosis is involved in a wide range of diseases, including cancer, neurodegeneration, ischemia/reperfusion (I/R)-induced tissue injury, metabolic diseases, immunological diseases and so on[19-22]. Additionally, ferroptosis has emerged as a significant and evolutionarily conserved regulator of aging, mediated through the interplay of lipid metabolism dysregulation, oxidative stress, and disrupted iron homeostasis[23-25]. The nematode *C. elegans*-a leading model for aging research-exhibits age-associated elevated iron levels, GSH depletion, and increased susceptibility to ferroptosis[23]. Treatment of liproxstatin-1, a potent ferroptosis inhibitor, could also significantly alleviate age-related cell death and substantially extend lifespan in *C. elegans.* This beneficial outcome could be attributable to the accumulation of MUFAs, which combats the age-related rise in lipid oxidation. This process enhances longevity by elevating the MUFAs/PUFAs ratio in the membrane lipids of *C. elegans*[26]. These findings offer novel opportunities for regulating longevity through lipid metabolism adjustments.

In this study, we identified VA and its analogues as potent ferroptosis inhibitors through high-throughput screening. Although VA and ATRA have previously been found as ferroptosis inhibitors[27], we unexpectedly discovered that the anti-ferroptotic activity of VA/ATRA is independent of the traditional RAR/RXR transcriptional signaling pathway. Instead, VA and its analogues bind to and activate ACSL3, facilitating the incorporation of MUFAs into phospholipids to inhibit ferroptosis. Additionally, we demonstrate that VA analogues significantly reduce aging-induced lipid peroxidation and extend lifespan in *C. elegans*. These findings unveil novel VA analogues that modulate lipid metabolism, thereby offering a promising strategy for modulating ferroptosis and promoting longevity.

2. Results

2.1. Vitamin A and its metabolites inhibit ferroptosis independent of antioxidant capacity or RAR/RXR activation

To discover small molecule compounds that inhibit ferroptosis, we performed a phenotypic screening against a compound library (∼4000) in HT-1080 cells (Supporting Information Fig. S1A)[28]. Notably, vitamin A (VA) and its metabolite all-*trans* retinoic acid (ATRA) were identified as ferroptosis inhibitors (Fig. S1B and Fig. 1A). VA is an essential nutrient, which is obtained from dietary sources including animals and plants, and ATRA is the most abundant and active metabolite of VA. The half maximal effective concentration (EC_{50}) of VA and ATRA in response to RSL3-induced ferroptosis were determined to be 0.40 and 3.78 μmol/L, respectively in HT-1080 cells (Fig. 1B). Similarly, for Erastin-induced ferroptosis, the EC_{50} values were 1.94 and 8.12 μmol/L for VA and ATRA, respectively (Fig. 1B). The efficacy of VA and ATRA in suppressing ferroptosis was comparatively lower than that of the well-established ferroptosis inhibitors Liproxstatin-1

(Lip-1) and Ferrostatin-1 (Fer-1) (Fig. S1C), which function as potent radical-trapping agents (RTAs) that directly scavenge lipid peroxides. Notably, however, the effective concentration of VA falls within the range of physiological serum retinol levels (1−3 μmol/L) observed under normal conditions[29]. VA and ATRA also efficiently rescued cells from ferroptosis triggered by RSL3 or Erastin in other cancer and non-cancer cell lines including 786-O, SK-HEP-1, 769-P and ARPE-19 cells (Fig. S1D−S1F). Intriguingly, we found that the intermediate metabolite retinal (RAL), which is essential for phototransduction in retina, also inhibited ferroptosis (Fig. 1C). In addition, VA, ATRA and RAL did not affect staurosporine (STS)-induced apoptosis and H_2O_2-induced necrosis (Fig. S1G), showing their specificity in ferroptosis inhibition. Moreover, VA, ATRA and RAL suppressed *GPX4*-knockout triggered ferroptotic cell death (Fig. 1D).

VA, ATRA and RAL efficiently reduced RSL3-or Erastin-induced lipid peroxidation-a hallmark of ferroptosis-in HT-1080 and 786-O cells in a concentration-dependent manner (Fig. S1H−S1L). However, unlike the antioxidant Trolox, these compounds do not act as radical-trapping agents (RTAs) as measured by the DPPH assay (Fig. 1E). This was further confirmed by fluorescence-enabled inhibited autoxidation (FENIX) assay, which employs liposomes composed of egg phosphatidylcholine to simulate the cell membrane's lipid bilayer *in vitro*. Compared to Fer-1, a well-established RTA, supplementation with ATRA and RAL up to 10 μmol/L did not significantly delay the process of autoxidation, while VA exhibited a modest inhibitory effect on autoxidation (Fig. 1F). These results suggest that the anti-ferroptotic effects of VA, ATRA and RAL are not attributed to direct antioxidative capabilities, while VA may act partially through modest antioxidant activity.

It has been well established that biological functions of VA/ATRA are mediated through downstream gene transcription, which is regulated by the RAR/RXR nuclear receptors[30,31]. However, VA and ATRA did not appear to influence the expression of those genes involved in ferroptosis regulation, including *ACSL4*, *GPX4*, *SLC7A11*, *FSP1*, *SCD1*, *HO-1* and *NRF2*, in HT-1080, 786-O or ARPE-19 cells (Fig. 1G, Supporting Information Fig. S2). VA and ATRA also did not alter cellular levels of glutathione (GSH), a co-substrate of GPX4 (Supporting Information Fig. S3A). Since ferroptosis is an iron-dependent cell death, we proceeded to investigate whether VA and ATRA regulate iron metabolism. The levels of labile ferrous iron, detected by FerroOrange, were not affected by VA or ATRA (Fig. S3B). Moreover, the expression of genes involved in iron metabolism, including *FTH1*, *TFRC* and *IRP1*, was not altered by either VA or ATRA in multiple cell lines (Fig. 1H and Fig. S2). These observations raise the possibility that VA and ATRA may suppress ferroptosis independently of *RAR/RXR*-mediated gene transcription. To investigate this intriguing hypothesis, we employed several pharmacological and genetic approaches. Firstly, we co-treated RSL3-challenged HT-1080 cells with VA/ATRA and a pan-RAR antagonist (AGN193109) or a pan-RXR antagonist (HX531). The results show that neither antagonist exerted a significant influence on the inhibitory effects of VA and ATRA on ferroptosis in HT-1080 cells (Fig. 1I, J and Fig. S3C). Similar results were also observed in 786-O and ARPE-19 cells (Fig. S3D and S3E). We also evaluated some other antagonists targeting RAR (BMS453, LE135 and LY2955303) or PPARβ/δ (GSK3787), and found these compounds did not affect the anti-ferroptotic activity of VA and ATRA either (Fig. S3F). Second, we constructed *RXRA* and *RXRB* knockout cells (Fig. S3G and S3H), and examined the effects of VA and ATRA on RSL3-induced ferroptosis. The results show that neither knockout of *RXRA* or *RXRB* individually nor *RXRA*/*RXRB* double knockdown affect the anti-ferroptosis activity of VA and ATRA (Fig. 1K, Fig. S3I and S3J). Third, we treated cells with Ch55 and ADA, two RAR agonists that are known to stimulate *RAR/RXR*-mediated gene transcription[32,33]. However, these two compounds did not exhibit inhibitory effect on ferroptosis (Fig. 1L). Consequently, these data demonstrate that inhibition of ferroptosis by VA and its metabolites is independent of *RAR/RXR* activation.

2.2. *A new class of VA analogues are identified as ferroptosis inhibitors*

We observed that VA and its metabolites ATRA and RAL are potent ferroptosis inhibitors, which is consistent with the previous findings[27,34]. However, their activities had not been impacted by *RAR/RXR* inactivation in our results. These findings prompt us to direct our attention to the structural characteristics of VA, ATRA, and RAL. Notably, we noticed that they all share a common structural motif, which possess a β-Ionone ring and a polyunsaturated side chain. To further clarify the significance of key structural determinants in VA, we designed and synthesized a series of VA analogues through optimization of the number of double bonds, the hydroxy group in VA, and carboxylic acid group in ATRA. The synthesis primarily commenced with commercially available VA, ATRA, and β-Ionone. These starting materials underwent a series of reactions including Wittig-Horner reactions, reduction, oxidation, esterification, and amide formation, ultimately yielding 16 analogues with the longest linear sequence consisting of 6 steps (Supporting Information Schemes S1−S3). The activities of these compounds against ferroptosis were measured in HT-1080 cells and a preliminary structure−activity relationship was established (Table 1). Our results suggest a positive correlation between the number of double bonds in these VA analogues and their anti-ferroptotic activity (Fig. 2A). Specifically, unsatisfactory anti-ferroptotic activity was observed in VA analogues A1 and B1-B5, which possess one or two double bonds (Table 1). Similarly, VA analogues C1−C3 embedded with three double bonds in their side chains did not exhibit improved activity. Interestingly, replacing the terminal functional groups of C1−C3 with a hydroxy group (C4), an aldehyde (C5), and a ketone (C6) significantly enhanced their anti-ferroptotic activity (Table 1). The side chains of the VA analogues D1−D4, 4-HRP, and Acitretin tethering four double bonds, were subsequently synthesized and evaluated. Notably, the presence of four conjugated double bonds, combined with optimized terminal functionalities-particularly hydroxy groups and related polar motifs-proved essential for effective ferroptosis inhibition. To our delight, all these compounds exhibited considerable anti-ferroptotic activity, with D3 being the most effective, demonstrating an excellent EC_{50} value of 0.53 μmol/L against RSL3-induced ferroptosis.

Similar to VA and ATRA, these analogues had no direct antioxidative property, as evidenced by DPPH assay (Fig. 2B) and FENIX assay (Fig. 2C). Moreover, the representative analogues C4, D2 and D3 efficiently suppressed RSL3-triggered lipid ROS accumulation, whereas C5 did not exhibit this effect (Fig. 2D), indicating C5 may possess a distinct activity to inhibit ferroptosis. To rule out the possibility that these analogues act through activating the RAR/RXR pathway, we utilized a RARE-luciferase reporter system. The results show that, in contrast to ATRA, a

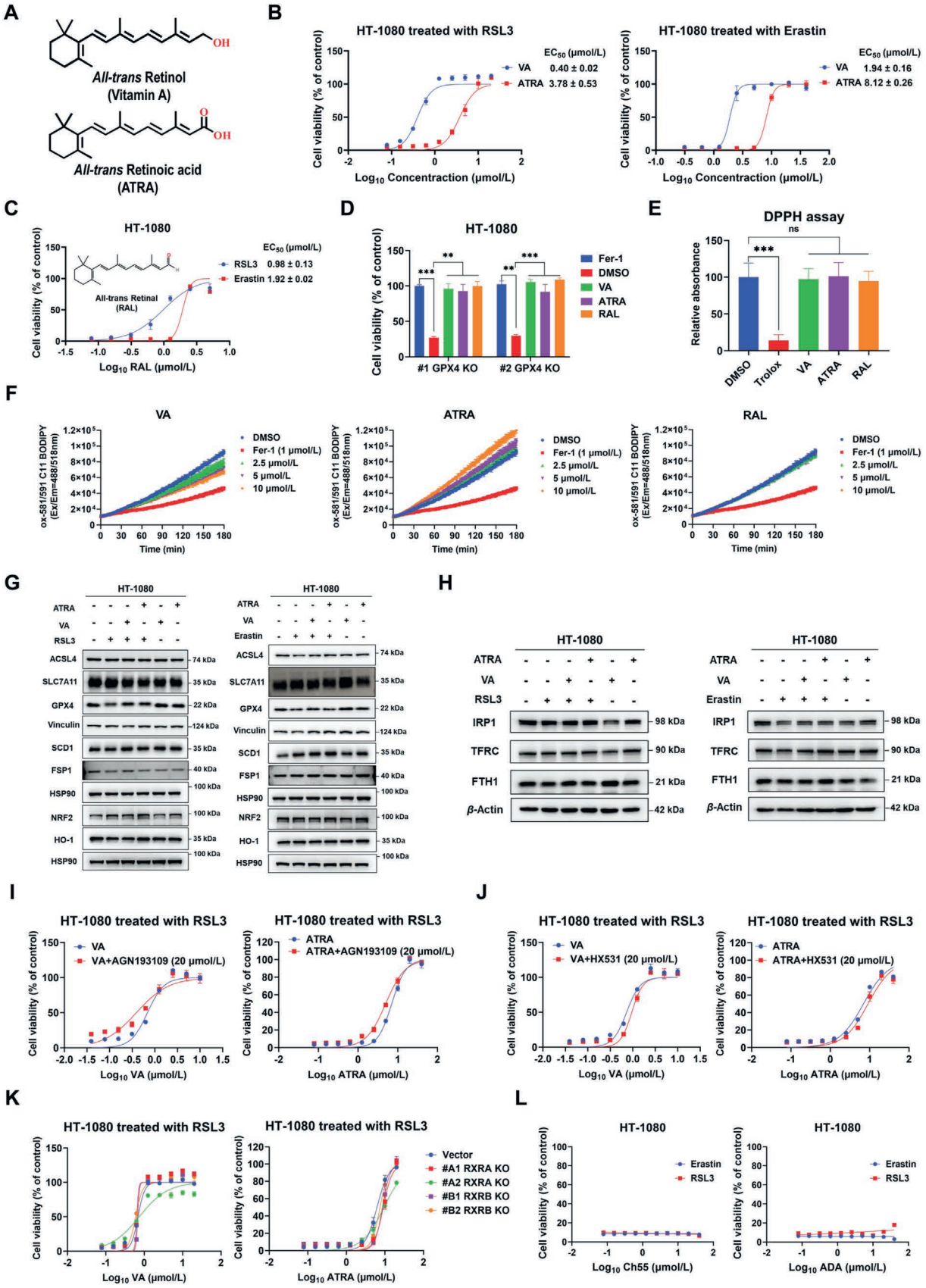

Figure 1 Vitamin A and its metabolites inhibit ferroptosis independent of antioxidant capacity or RAR/RXR activation. (A) Illustration of the structures of VA and ATRA. (B) Measurement of the EC_{50} values of VA and ATRA towards RSL3 (0.5 μmol/L) or Erastin (10 μmol/L) induced ferroptosis in HT-1080 cells. Cells were treated with drugs for 24 h. (C) RAL suppressed RSL3 and Erastin-induced ferroptosis in HT-1080 cells.

Table 1 The activities of VA analogues against ferroptosis in HT-1080 cells.

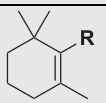

Compd.	R	EC_{50} (RSL3, μmol/L)	EC_{50} (Erastin, μmol/L)	Antioxidant capacity (DPPH)
A1		>40	>40	No
B1	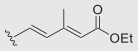	>40	>40	No
B2	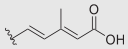	>40	>40	No
B3	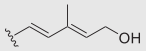	>15.54	>30.49	No
B4	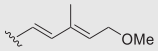	>40	>40	No
B5	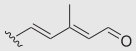	>30.88	>22.37	No
C1	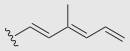	>40	>40	No
C2	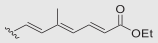	14.17	>40	No
C3	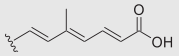	>40	>40	No
C4	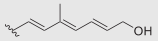	1.18	3.38	No
C5	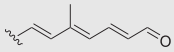	2.48	13.14	No
C6	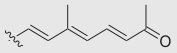	7.83	>27.97	No
D1	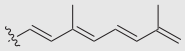	2.23	>40	No
D2	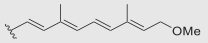	2.82	7.08	No
D3	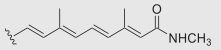	0.53	7.98	No
D4	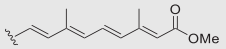	4.96	31.30	No
4-HRP	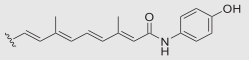	0.61	3.30	No
Acitretin	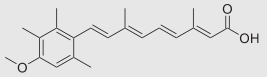	2.98	17.53	No

renowned ligand for RAR/RXR signaling, none of the analogues B3, B5, C5, C6, D2 or D3 were able to activate RARE-driven luciferase expression (Fig. 2E). This experiment reinforces the conclusion that VA and its analogues inhibit ferroptosis independent of the RAR/RXR signaling. Taken together, these observations demonstrate that VA and its analogues exert their anti-ferroptotic function through similar structural features rather than by promoting gene transcription.

(D) Viability of HT-1080 *GPX4*-KO cells treated with the indicated compounds for 24 h after withdrawal of Fer-1, which is essential for the survival of *GPX4*-KO cells. (E) The antioxidative capacity of VA (50 μmol/L), ATRA (50 μmol/L) and RAL (50 μmol/L) was analyzed by the DPPH (2,2-diphenyl-1-picrylhydrazyl) assay. Trolox (50 μmol/L) was used as a positive control. (F) The effect of VA, ATRA and RAL on the autoxidation of C11 $BODIPY^{581/591}$ initiated by AAPH in EggPC liposomes was measured by FENIX assay. Fer-1 was used as a positive control. (G) Protein expression levels of GPX4, SLC7A11, ACSL4, SCD1, FSP1, HO-1 and NRF2 in HT-1080 cells were analyzed by Western blot. Cells were treated with VA (1 μmol/L) or ATRA (10 μmol/L) in the presence or absence of RSL3 (0.25 μmol/L) for 2.5 h or Erastin (10 μmol/L) for 8 h. (H) Protein expression levels of IRP1, TFRC and FTH1 in HT-1080 cells were analyzed by Western blot. Cells were treated with VA (1 μmol/L) or ATRA (10 μmol/L) in the presence or absence of RSL3 (0.25 μmol/L) for 2.5 h or Erastin (10 μmol/L) for 8 h. (I, J) Cell viability of HT-1080 cells after co-treatment with RSL3 and VA or ATRA in the presence of pan-RAR antagonist AGN193109 (20 μmol/L) (I) or pan-RXR antagonist HX531 (20 μmol/L) (J). (K) The protective effects of VA or ATRA on RSL3-induced ferroptosis in RXRA and RXRB knockout HT-1080 cells. (L) Viability of HT-1080 cells treated with different doses of RAR agonists Ch55 and Adapalene (ADA) under RSL3 (0.5 μmol/L) and Erastin (10 μmol/L)-induced ferroptosis for 24 h. Data shown represent the mean ± SD ($n = 3$). $^{**}P < 0.01$, and $^{***}P < 0.001$, indicating significant differences between groups. ns means no significance.

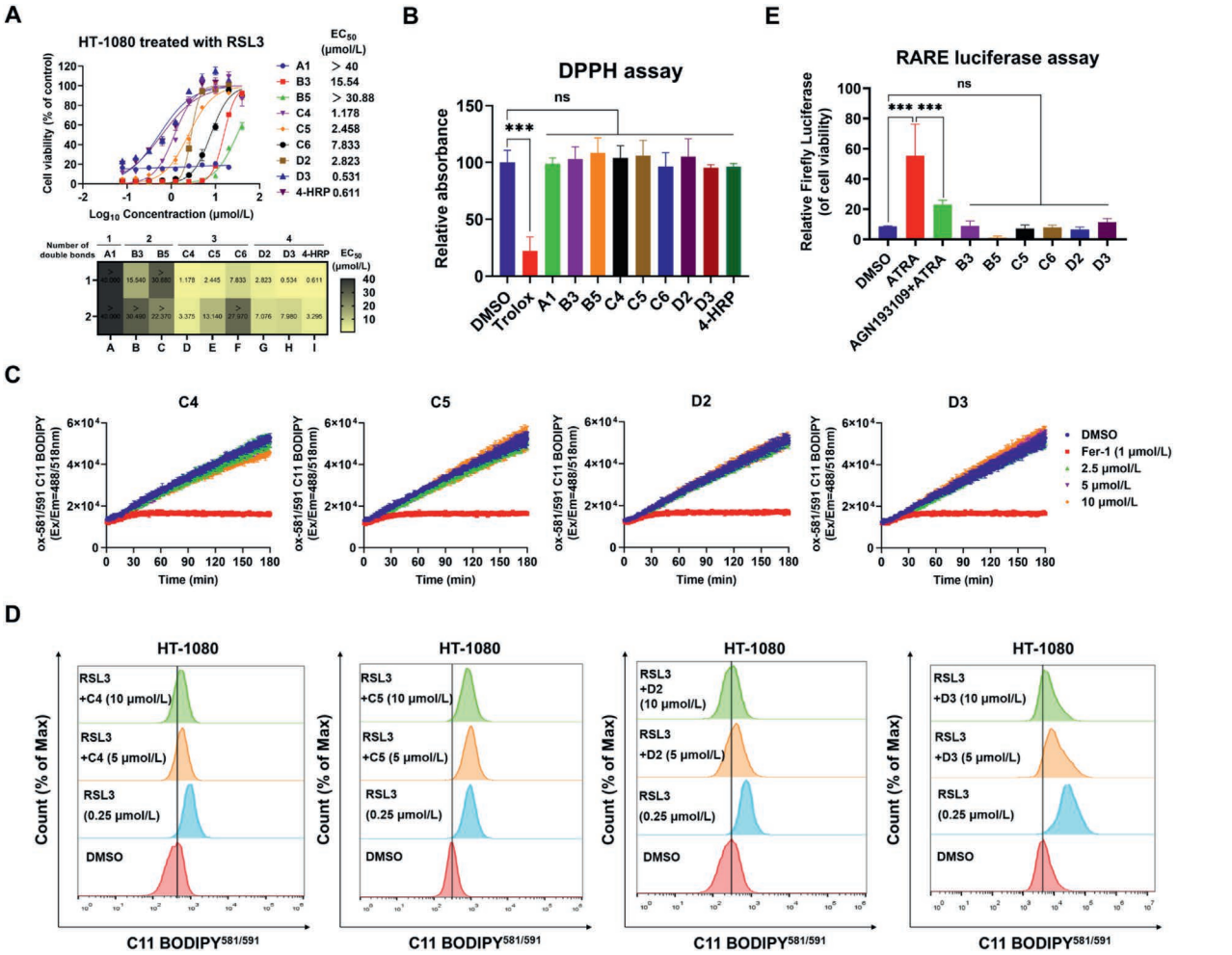

Figure 2 VA analogues inhibit ferroptosis. (A) Measurement of the EC_{50} values of VA analogues towards RSL3-induced ferroptosis in HT-1080 cells. The heatmap illustrates the EC_{50} values of VA analogues. ">" indicates that EC_{50} is greater than the marked value. (B) VA analogues did not possess antioxidative activity measured by DPPH assay. Trolox (50 μmol/L) was used as a positive control. (C) VA analogues did not suppress autoxidation of C11 BODIPY$^{581/591}$ initiated by AAPH in EggPC liposomes. Fer-1 was used as a positive control. (D) Lipid peroxidation evaluated by C11 BODIPY$^{581/591}$ staining in HT-1080 cells. (E) VA analogues did not activate RARE luciferase activity. HEK293T cells transfected with pGL3-RARE were pretreated with RAR antagonist (AGN193109), and then treated with ATRA (10 μmol/L), B3 (20 μmol/L), B5 (20 μmol/L), C5 (10 μmol/L), C6 (10 μmol/L), D2 (10 μmol/L) and D3 (5 μmol/L) for 24 h. Luciferase activity was assayed. The results are expressed as relative value of luciferase activity to cell viability. Data shown represent the mean ± SD ($n = 3$). ***$P < 0.001$, indicating significant differences between groups. ns means no significance.

2.3. VA and its analogues protect against ConA-induced acute liver injury and hepatic ischemia/reperfusion (I/R) injury

Since VA and its analogues had a pronounced inhibitory activity against ferroptosis *in vitro*, we further investigated their protective effects against ferroptosis-related pathology *in vivo*. The liver serves as the primary organ for VA storage, where hepatic stellate cells (HSCs) store approximately 80% of VA. Consequently, the ferroptosis inhibition by VA and its analogues may possess clinical potential for the treatment of liver-related diseases[35]. Previous studies indicate that Concanavalin A (ConA) is known to induce ferroptosis in mouse liver, causing acute liver injury (ALI), which could be alleviated by ferroptosis inhibitors[28,36,37]. When VA, ATRA and D3 were applied on this model, all the three compounds compromised the elevated levels of serum alanine aminotransferase (ALT) and aspartate aminotransferase (AST) induced by ConA (Fig. 3A and B). H&E staining of mouse liver sections indicated that treatments with VA, ATRA and D3 significantly alleviated ConA-induced acute liver injury in mice (Fig. 3C). Moreover, treatment with VA, ATRA and D3 reduced the levels of lipid peroxidation markers, including 4-HNE (Fig. 3C), MDA (Fig. 3D), and restored GPX4 expression level that was reduced by ConA (Fig. 3E). Meanwhile, VA, ATRA and D3 decreased the hepatic iron level (Fig. 3C), *Ptgs2* expression (Fig. 3F), as well as inflammatory factor *Tnfα* expression in mouse liver (Fig. 3G). Hepatic ischemia/reperfusion (I/R) injury is another well-recognized pathological process that involves ferroptosis[38,39] and represents a major challenge in liver transplantation. Intriguingly, treatment with VA or D3 significantly compromised the hepatic I/R-induced elevation of serum ALT and AST levels (Fig. 3H). H&E staining showed that hepatic injury was mitigated in mice with VA or D3 treatment (Fig. 3I). Moreover, VA or D3

also reduced the hepatic iron deposition (Fig. 3I), *Ptgs2* expression (Fig. 3J) and rescued GPX4 downregulation (Fig. 3K) induced by I/R injury. Together, these results suggest that VA and its analogues effectively alleviate ConA-induced ALI and hepatic IR injury through inhibition of ferroptosis.

2.4. ACSL3 is required for VA analogues-induced protection from ferroptosis

To identify the molecular targets of VA and its analogues, we performed the limited proteolysis mass spectrometry (Lip-MS) profiling (Fig. 4A). Among 75 candidate proteins identified, we prioritized ACSL3, PRDX6, and TXNRD1 based on their established roles in lipid metabolism and redox regulation (Fig. 4B). Genetic validation using sgRNA-mediated knockout revealed that the anti-ferroptotic activity of VA was specifically dependent on ACSL3, as PRDX6-or TXNRD1-deficient cells maintained full responsiveness to VA treatment (Supporting Information Fig. S4A and S4B). Subsequently, *ACSL3* knockout monoclonal cells were generated in both 786-O and HT-1080 cells (Fig. 4C). In accordance with previous findings[15], *ACSL3* KO resulted in a modest increase in cellular vulnerability to ferroptosis (Fig. 4D). Notably, loss of *ACSL3* significantly attenuated the anti-ferroptotic effect of VA, ATRA and D3 analogue in 786-O and HT-1080 cells (Fig. 4E and F). Furthermore, the anti-ferroptotic effects of other VA analogues, such as 4-HRP and Acitretin, were also reduced in *ACSL3* KO cells (Fig. S4C and S4D). Consistent with these observations, VA, ATRA and D3 were not able to efficiently scavenge RSL3-induced lipid peroxidation in *ACSL3*-deficient 786-O and HT-1080 cells (Fig. 4G and H). Moreover, reconstitution of *ACSL3* in *ACSL3* KO cells restored the anti-ferroptotic effects of VA, ATRA and D3 (Fig. 4I and J). Taken together, the above findings indicate that *ACSL3* is indispensable for ferroptosis inhibition by VA and its analogues.

2.5. VA analogues inhibit ferroptosis through the regulation of MUFAs metabolism

ACSL3 catalyzes the activation of fatty acids to their acyl-CoA esters in the presence of ATP and CoA. This process is essential for the anti-ferroptotic activity of MUFAs, as it facilitates the incorporation of MUFA-CoA into PLs, thereby reducing the levels of PUFA-PLs[15]. This raises a possibility that VA analogues may regulate ACSL3 activity and affect the incorporation of MUFAs into phospholipids to suppress ferroptosis. To test this, we conducted targeted lipidomics analysis in HT-1080 cells treated with DMSO, VA, or D3. Intriguingly, both VA and D3 treatment significantly increased the MUFA/PUFA ratio in key membrane phospholipids (PEs and PCs) (Fig. 5A and B), indicating that MUFAs metabolism is involved in ferroptosis inhibition of VA analogues.

Given the structural similarity between the polyene chain of VA analogues and the fatty acid chain of unsaturated fatty acids, two hypotheses were proposed: (1) VA analogues might serve as direct substrates for ACSL3, leading to the formation of acyl-CoA ester-conjugated metabolites that could reduce PUFA-PLs in a manner similar to MUFA-CoA; (2) VA analogues might bind to ACSL3 and promote its activity. To clarify these hypotheses, we first explored whether inhibition of SCD1 would influence the activity of VA analogues. SCD1 catalyzes the desaturation of saturated fatty acids, principally stearic acid (18:0) and palmitic acid (16:0), to their D9-monounsaturated counterparts oleic acid (18:1) and palmitoleic acid (16:1)[40], thus providing MUFAs as substrates for ACSL3. As shown in Fig. 5C, pretreatment with SCD1 inhibitor A939572 decreased the protective effects of VA and ATRA against ferroptosis. To further confirm the results, we constructed *SCD1* knockout cells in HT-1080 cells (Fig. 5D). Knockout of *SCD1* led to a decrease of OA-CoA levels (Fig. 5E), indicating that *SCD1* deficiency decreased cellular MUFAs level, consequently reducing ACSL3-catalyzed OA-CoA synthesis. Consistent with a previous study[18], knockout of *SCD1* made cells more sensitivity to ferroptosis (Fig. 5F and Fig. S4E). Notably, loss of *SCD1* also significantly compromised the anti-ferroptotic activity of VA, ATRA and D3 (Fig. 5G and Fig. S4F), while this effect could be restored by the supplementation with oleic acid, a product synthesized by SCD1 (Fig. 5H and I). These results demonstrate that the anti-ferroptotic activity of VA analogues require SCD1 catalyzed MUFAs production. Thus, VA analogues are unlikely to be direct substrates of ACSL3.

2.6. VA analogues directly bind to ACSL3 and activate ACSL3

We then focused on investigating the hypothesis that VA analogues might directly or indirectly modulate ACSL3 activity. To this end, we synthesized a probe D5, an alkynyl-modified derivative of D3, for click-chemistry-based pull-down assay (Fig. 6A). D5 exhibited comparable anti-ferroptotic activity to D3 (Fig. 6B), confirming that alkynyl modification preserved biological function. Using this probe, we performed pull-down assays and successfully captured ACSL3, while pretreatment with high dosage of D3 competitively inhibited the interaction between D5 and ACSL3 (Fig. 6C), demonstrating specific binding between VA analogues and ACSL3. To further confirm the binding between VA analogues and ACSL3, we carried out a microscale thermophoresis (MST) assay by using labelled recombinant His-ACSL3 protein (Fig. 6D) along with a range of dilutions of VA analogues. The result also demonstrated the association between ACSL3 and VA, ATRA or D3 with dissociation constant (K_d) determined to be 1.85 μmol/L for VA, 12.82 μmol/L for ATRA, and 1.28 μmol/L for D3, respectively (Fig. 6E).

We then inquired about how VA analogues might regulate the function of ACSL3. As shown in Fig. 6F and G, VA and ATRA did not alter the expression levels of *ACSL3* mRNA and protein. Considering the increased ratio of MUFA/PUFA lipids (Fig. 5A), it is possible that VA analogues promote ACSL3 enzyme activity. In fact, VA analogues promoted acylation reaction with OA as substrate in the presence of ACSL3 (Fig. 6H), indicating ACSL3 enzyme activity were upregulated by VA analogues. To further clarify the binding modes of VA analogues with its target ACSL3, a protein structure-based molecular docking study was conducted using the predicated structure of ACSL3. VA analogues were successfully docked into the predicated binding pockets of ACLS3 (Fig. 6I). The binding energy (ΔG) data were shown in Supporting Information Table S1. These compounds established hydrogen bond interactions with Ser288, implying that Ser288 may be essential for VA analogues binding to ACSL3. We therefore re-expressed wildtype (WT) and mutant $ACSL3^{S288A}$ in *ACSL3* knockout cells (Fig. 6J). Both WT and mutant *ACSL3* were able to restore the reduced cell sensitivity to RSL3 caused by *ACLS3* KO, although the mutant *ACSL3* was not as efficient as the WT *ACSL3* in this regard (Fig. 6L). Notably, in comparison with *ACSL3*-WT, $ACSL3^{S288A}$ reconstitution failed to restore the anti-ferroptotic effect of VA, ATRA and D3 (Fig. 6K), indicating that Ser288

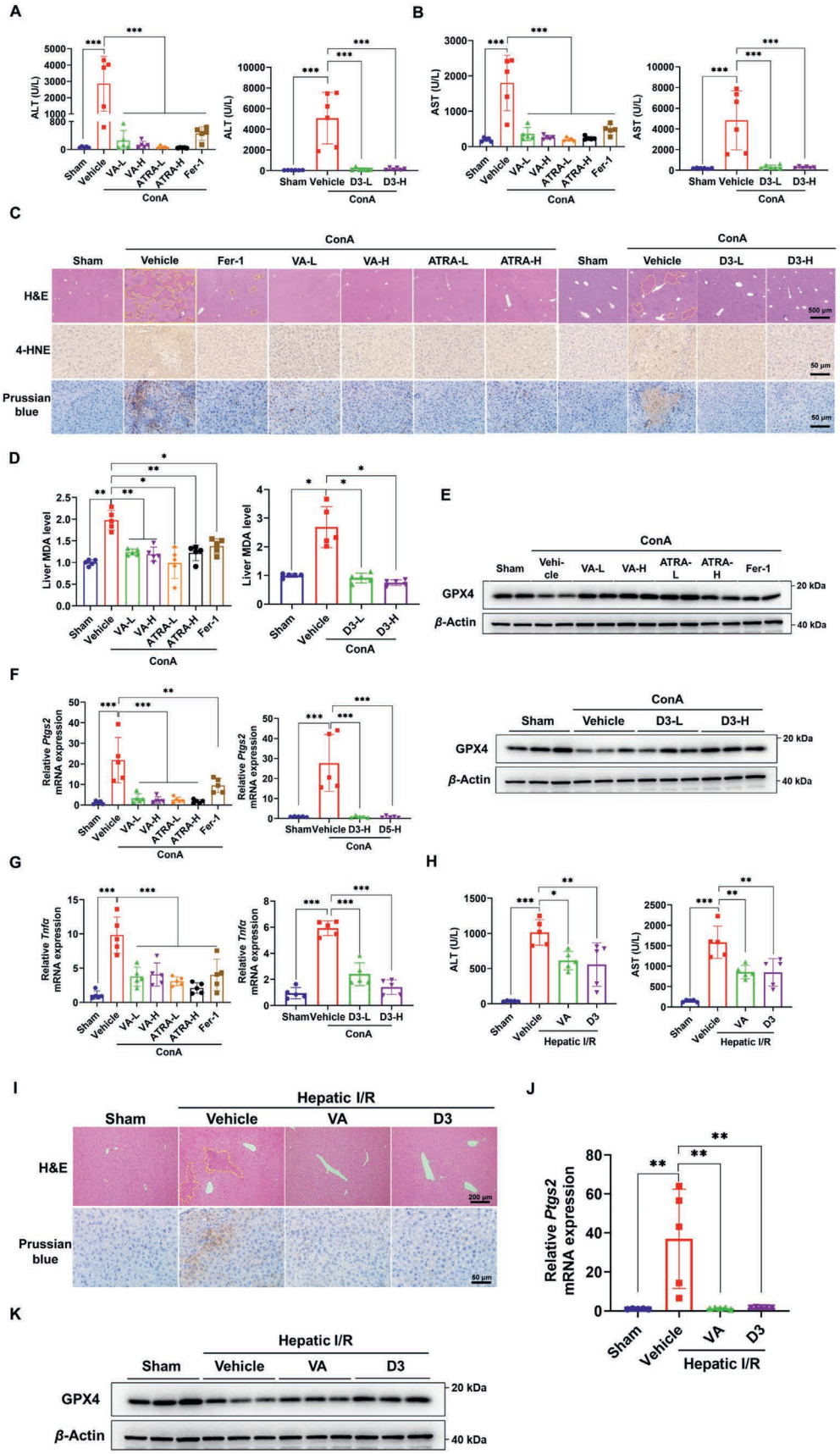

Figure 3 VA and its analogues attenuate ConA-induced acute liver injury and hepatic I/R injury through ferroptosis inhibition. (A, B) Concentrations of ALT (A) and AST (B) in mouse serum were measured with an automatic biochemical analyzer. H and L indicate high (30 mg/kg)

residue of *ACSL3* is required for VA analogues to suppress ferroptosis.

2.7. VA and its analogue D3 promote lifespan extension via ACSL3 homologous in C. elegans

Recent work shows that MUFAs increase lipid droplet abundance and reduce lipid oxidation during aging, further extending lifespan in *C. elegans*[26]. Meanwhile, ACS-4 and ACS-17, the *C. elegans* protein homologous to human ACSL3, are also localized on the surface of lipid droplets[41]. In light of these findings, we asked whether VA and its analogues may promote longevity *via* the regulation of MUFAs metabolism. Since loss-of-function (*lf*) of *acs-4(ok2872)* mutant displays a strong sterile phenotype while *acs-17(ok1562)* mutant is superficially wild-type, we knocked down (*kd*) *acs-4* in *acs-17(lf)* strains in case they are functionally redundant. In line with previous studies, we observed that middle-aged worms exhibited higher levels of malondialdehyde (MDA), a reliable biochemical marker of lipid peroxidation, compared to their younger counterparts (Fig. 7A and B). Treatment with VA or its analogue D3 reduced lipid oxidation in wild-type individuals, while these effects were diminished in the *acs-4(kd);acs-17(lf)* group (Fig. 7A and B). Notably, either VA or D3 treatment were found to significantly extended the worms' lifespan, an effect that was significantly compromised by *acs-4/17* deficiency (Fig. 7C and D, Supporting Information Table S2). To better understand how VA and D3 delay aging, we examined two key biomarkers of senescence: lipofuscin accumulation and senescence-associated β-galactosidase (SA-β-gal) activity[42,43]. We found that both VA and D3 treatments reduced lipofuscin accumulation in wild-type worms. However, this effect was largely compromised in the *acs-4(kd);acs-17(lf)* group (Fig. 7E and F). Similarly, VA and D3 decreased the area of SA-β-gal staining in wild-type worms on Day 7, an effect that was also not observed in the *acs-4(kd);acs-17(lf)* mutants (Fig. 7G and H). These observations indicate that ACSL3 homolog proteins are crucial for the activity of VA analogues in preventing lipid oxidation, and extending lifespan of *C. elegans*.

We next used a transgenic strain that expresses lipid droplet membrane protein DHS-3 fused with green fluorescent protein (GFP) to assess the number of lipid droplets *in vivo*[44,45]. DHS-3GFP is driven by the endogenous *dhs-3* promoter, which is expressed mainly in intestinal cells and localized to intestinal lipid droplets. In accordance with their lifespan-extending effects, both VA and D3 supplementation increased the number of lipid droplets in the intestine, the main fat storage tissue in *C. elegans*, while this effect was abolished in *acs-4(kd);acs-17(lf)* group (Fig. 7I and J). In particular, *acs-4(kd);acs-17(lf)* worms were strongly inhibited in locomotion and whose phenotype like paralysis, suggesting that reduced lipid droplets may be related to locomotion. To further evaluate the importance of each ACSL3 homolog protein in mediating the function of VA and D3 in lifespan extension, we knocked down either *acs-4* or *acs-17*, respectively. The results show that degradation of *acs-4(kd)* had a greater impact on diminishing VA or D3-promoted longevity than *acs-17 (kd)* (Fig. 7K and L), indicating *acs-4* is the major contributor in mediating the function of VA or D3. Together, these data suggest that VA and D3 extend lifespan through regulation MUFA metabolism to reduce lipid peroxidation *via* ACSL3 homolog proteins in *C. elegans*.

3. Discussion

VA is an essential micronutrient that must be obtained from the diet, which is subsequently metabolized into retinal (RAL) and retinoic acid (ATRA). VA and its metabolites are indispensable for systemic health, playing critical roles in embryonic development, visual function, metabolic homeostasis, and immune regulation, among other vital physiological processes[46]. It is widely accepted that ATRA, the predominant active metabolite of VA, acts as a ligand for the RAR/RXR nuclear receptor complex, leading to its activation and subsequent modulation of gene expression. While ATRA has been reported to influence non-genomic signaling pathways[47-49], the activity of VA and ATRA that is independent of transcriptional control remains largely unexplored. In the current study, we uncovered a novel activity of VA and its analogues that binds and activates ACSL3 to regulate lipid metabolism. Consistent with the function of ACSL3 in protecting cells from ferroptosis, we observed VA and those analogues suppressed ferroptosis at concentrations resembling physiological levels. This activity is contingent upon the polyene chain present in the structure of these compounds, as those containing four double bonds in side chain, resembling the structure of VA, demonstrated the most potent activity against ferroptosis. In recent years, vitamin family members have been found to possess new functions beyond their traditional activities[50-52]. Our current study also provides important clues regarding new functions of vitamin A beyond transcriptional regulation.

Several previous studies have suggested that VA possesses antioxidant properties[53,54]. However, there has been a long-lasting debate concerning whether VA and ATRA exerts its antioxidant effects directly or indirectly[55]. Although some studies have suggested that VA and RAL may inhibit ferroptosis through antioxidative activity[27,34], our findings from DPPH, ABTS, and FENIX assays consistently reveal that VA and its metabolites possess minimal radical-trapping activity. Furthermore, the newly synthesized VA analogues that have anti-ferroptotic activity also lack antioxidant properties. This suggests that VA and its analogues mitigate ferroptosis *via* indirect mechanisms rather than through direct radical scavenging. Based on the current understanding, the biological activity of VA/ATRA is primarily ascribed to RAR/RXR mediated gene transcription[30]. Recent studies suggested that ATRA activates RAR/RXR to transcriptionally

and low (10 mg/kg)) concentration of drugs, respectively. (C) Representative images of H&E staining, 4-HNE immunostaining and DAB-enhanced Prussian blue staining in mouse liver sections. Lesions observed in the livers were indicated by yellow lines. Scale bars: 200 or 50 μm. (D) MDA levels in liver tissues were measured by a biochemical kit. (E) Western blot analysis of GPX4 protein in the liver of ConA-induced ALI. (F) The relative mRNA expression of *Ptgs2* in mouse livers. *Gapdh* served as an endogenous control. (G) The relative mRNA expression of *Tnfα* in mouse livers. *Gapdh* served as an endogenous control. (H) Serum levels of ALT and AST were assessed by an automatic biochemical analyzer. The dosage of VA and D3 is 15 mg/kg. (I) Liver sections were stained with H&E staining and DAB-enhanced Prussian blue staining. Lesions observed in the livers were indicated by yellow lines. Scale bars: 200 or 50 μm. (J) Hepatic *Ptgs2* mRNA expression was assessed by qRT-PCR. (K) Western blot analysis of GPX4 protein in the liver of hepatic I/R injury. Data shown represent the mean ± SD ($n = 5$). $^{*}P < 0.05$, $^{**}P < 0.01$, and $^{***}P < 0.001$, indicating significant differences between groups.

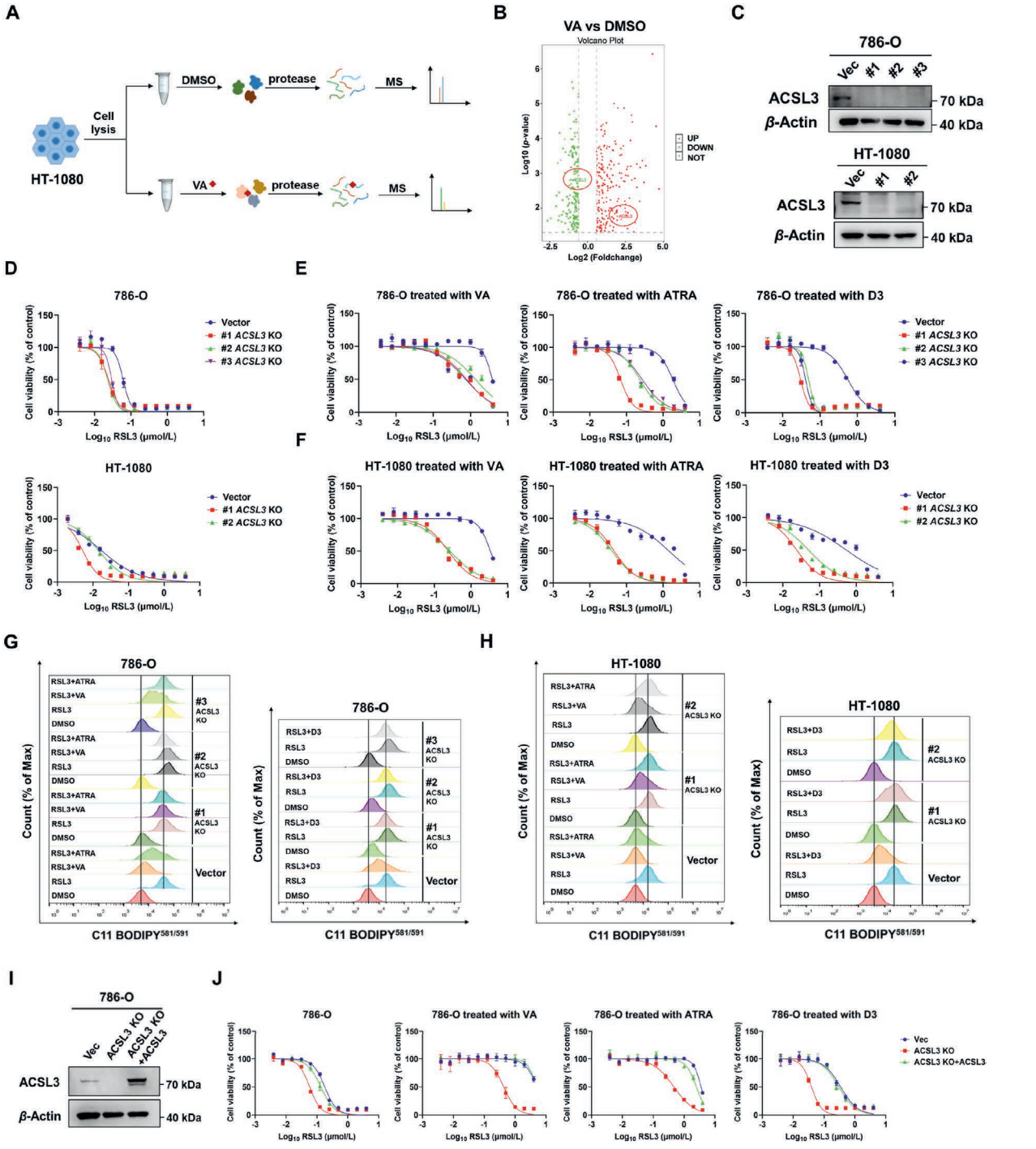

Figure 4 ACSL3 is required for VA analogues-induced protection from ferroptosis. (A) The work flow of Lip-MS assay. (B) Volcano plots of feature sequence in Lip-MS assay. ACSL3 emerged as a potential target of VA. (C) Validation of *ACSL3* KO in 786-O and HT-1080 cells. (D) Viability of vector and *ACSL3* KO 786-O and HT-1080 cells treated with different dosages of RSL3 for 24 h. (E, F) *ACSL3* KO compromised the anti-ferroptotic effect of VA analogues in (E) 786-O and (F) HT-1080 cells. Cells were co-treated with RSL3 (0.5 μmol/L) and VA (1 μmol/L), ATRA (10 μmol/L) or D3 (2 μmol/L) for 24 h. (G, H) Lipid peroxidation evaluated by C11 BODIPY$^{581/591}$ staining in vector and *ACSL3* KO 786-O (G) and HT-1080 (H) cells. (I) Validation of ectopically expressed ACSL3 in *ACSL3* KO 786-O cells by Western blot. (J) Reconstitution of *ACSL3* in *ACSL3* KO cells restored the protective effects of VA analogues against ferroptosis. Cells were co-treated with RSL3 (0.5 μmol/L) and VA (1 μmol/L), ATRA (10 μmol/L) or D3 (2 μmol/L) for 24 h. All the data are presented as the mean ± SD (n = 3).

upregulate a bunch of ferroptosis-protective genes including *GPX4*, *FSP1*, *GCH1*, *ACSL3* and *SCD1*[27,34]. However, by employing a comprehensive strategy involving the use of pan-RAR antagonists, pan-RXR antagonists, RAR agonists and *RXR* gene knockout models, we have proven that neither suppression nor activation of RAR/RXR signaling influenced the protective effects of VA and ATRA against ferroptosis (Fig. 1). Moreover, newly synthesized VA analogues, which displayed potent

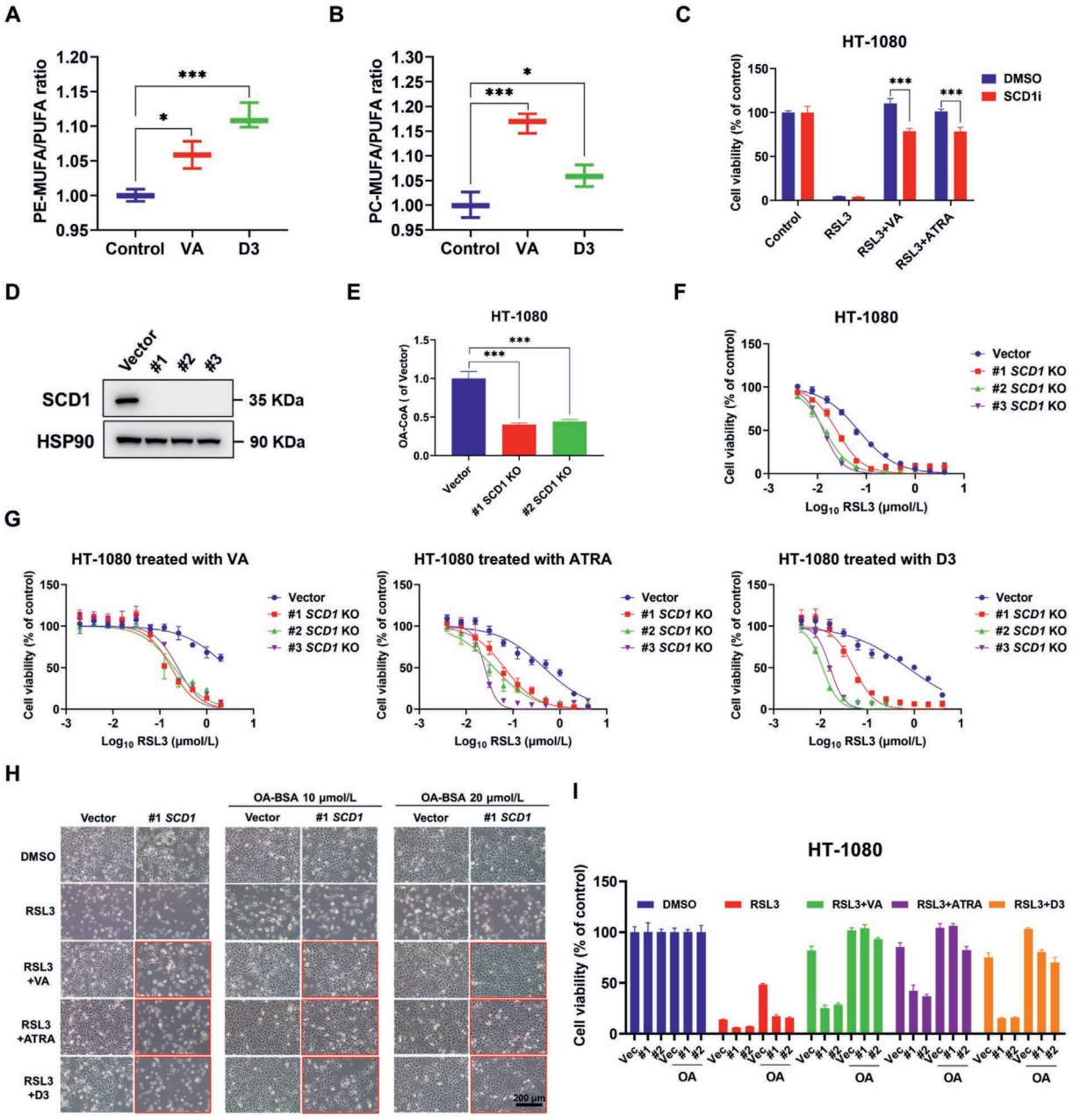

Figure 5 VA analogues inhibit ferroptosis through the regulation of MUFA metabolism. (A, B) Lipidomic analysis of MUFAs and PUFAs in membrane lipids including PE (A) and PC (B) following VA (5 μmol/L) and D3 (5 μmol/L) treatment for 12 h in HT-1080 cells. (C) Viability HT-1080 cells treated with RSL3 (0.5 μmol/L) and VA (1 μmol/L) or ATRA (10 μmol/L) in the presence or absence of SCD1 inhibitor A939572 (20 μmol/L) for 24 h. (D) Validation of *SCD1* KO in HT-1080 cells. (E) The levels of OA-CoA were decreased in *SCD1* knockout HT-1080 cells. (F) Viability of Vector and *SCD1* KO cells treated with RSL3 for 24 h. (G) *SCD1* KO compromised the anti-ferroptotic effect of VA analogues in HT-1080 cells. Cells were treated with RSL3 (0.5 μmol/L) and VA (1 μmol/L), ATRA (10 μmol/L) or D3 (5 μmol/L) for 24 h. (H, I) Supplement of OA restored the protective effect of VA analogues against ferroptosis. Vector and *SCD1* KO HT-1080 cells were pretreated with OA in (10 and 20 μmol/L in panel H, and 10 μmol/L in panel I, followed by treatment with RSL3 (0.5 μmol/L) and VA (1 μmol/L), ATRA (10 μmol/L) or D3 (5 μmol/L) for 24 h. All the data are presented as the mean ± SD ($n = 3$). $^{*}P < 0.05$, $^{***}P < 0.001$, indicating significant differences between groups.

inhibitory effect on ferroptosis, were not able to activate RARE mediated gene transcription (Fig. 2E). These results provide compelling evidence that the inhibitory effect of VA and its analogues on ferroptosis operates independently of the RAR/RXR signaling pathway.

Inspired by the similar polyene chain of VA analogues, we discovered that these compounds actually bind to ACSL3 and enhance its enzyme activity, thereby increasing the MUFA/PUFA-PLs ratio to inhibit ferroptosis. Previous studies indicate that ACSL3 is required for the extracellular lipid utilization and

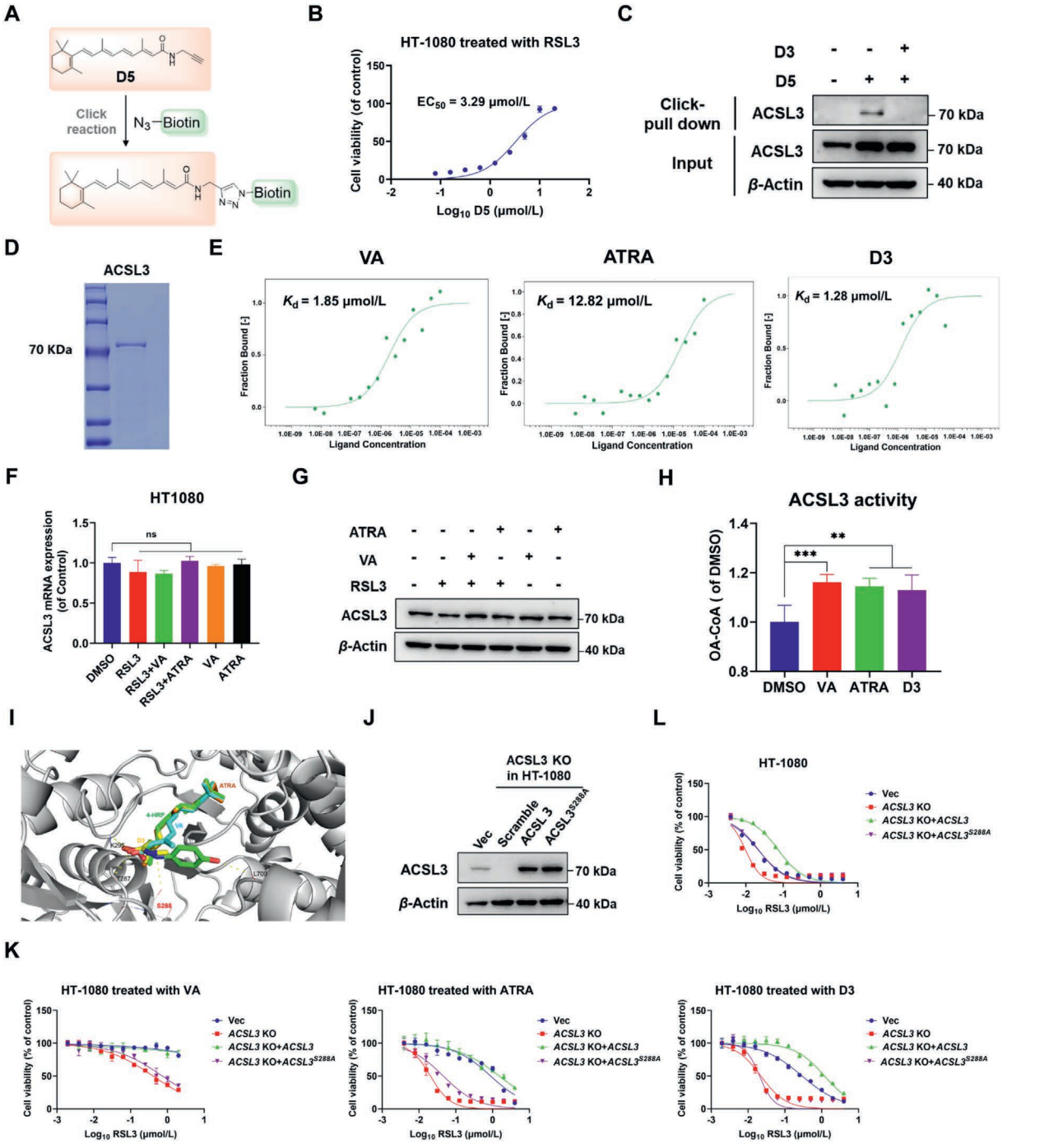

Figure 6 VA analogues directly bind to ACSL3 and activate ACSL3. (A) The flow diagram of D5-probe pull-down assay *via* a click chemistry reaction. (B) D5-probe suppressed RSL3-induced ferroptosis in HT-1080 cells. (C) D5-probe was able to pull down ACSL3 from cell lysates, which could be competitively abolished by D3. HT-1080 cell lysates were incubated with D5-probe (5 μmol/L) in the presence or absence of a 10-fold excess of unlabeled D3 (50 μmol/L), followed by click pull-down with streptavidin-agarose. (D) Purification of human ACSL3 protein. (E) Binding of VA, ATRA or D3 to ACSL3 protein was analyzed by a microscale thermophoresis (MST) assay. (F, G) VA and ATRA did not affect either the mRNA (F) or protein (G) level of ACSL3. HT-1080 cells were treated with VA (1 μmol/L) or ATRA (10 μmol/L) in the presence or absence of RSL3 (0.25 μmol/L) for 2.5 h. (H) VA, ATRA, and D3 enhanced the enzymatic activity of ACSL3. The activity of ACSL3 in catalyzing the production of OA-CoA was measured using LC−MS. (I) Representative docking patterns of VA analogues into the predicted binding sites of ACSL3 using Autodock Vina. All the structure figures were produced with PyMOL. VA (blue), ATRA (orange), D3 (yellow) and 4-HRP (green) were presented in the docking models. (J) Validation of ectopically expressed *ACSL3*-WT or $ACSL3^{S288A}$ in *ACSL3* KO HT-1080 cells by Western blot. (K) Reconstitution of $ACSL3^{S288A}$ failed to restore the protective effect of VA analogues against ferroptosis. Cells were co-treated with RSL3 (0.5 μmol/L) and VA (1 μmol/L), ATRA (10 μmol/L) or D3 (5 μmol/L) for 24 h. (L) *ACSL3* KO HT-1080 cells transfected with vector, *ACSL3*-WT and $ACSL3^{S288A}$ were treated with RSL3 and the cell viability was detected by CellTiter-Glo. All the data are presented as the mean ± SD. $^{*}P < 0.05$, $^{**}P < 0.01$, $^{***}P < 0.001$, indicating significant differences between groups. ns means no significance.

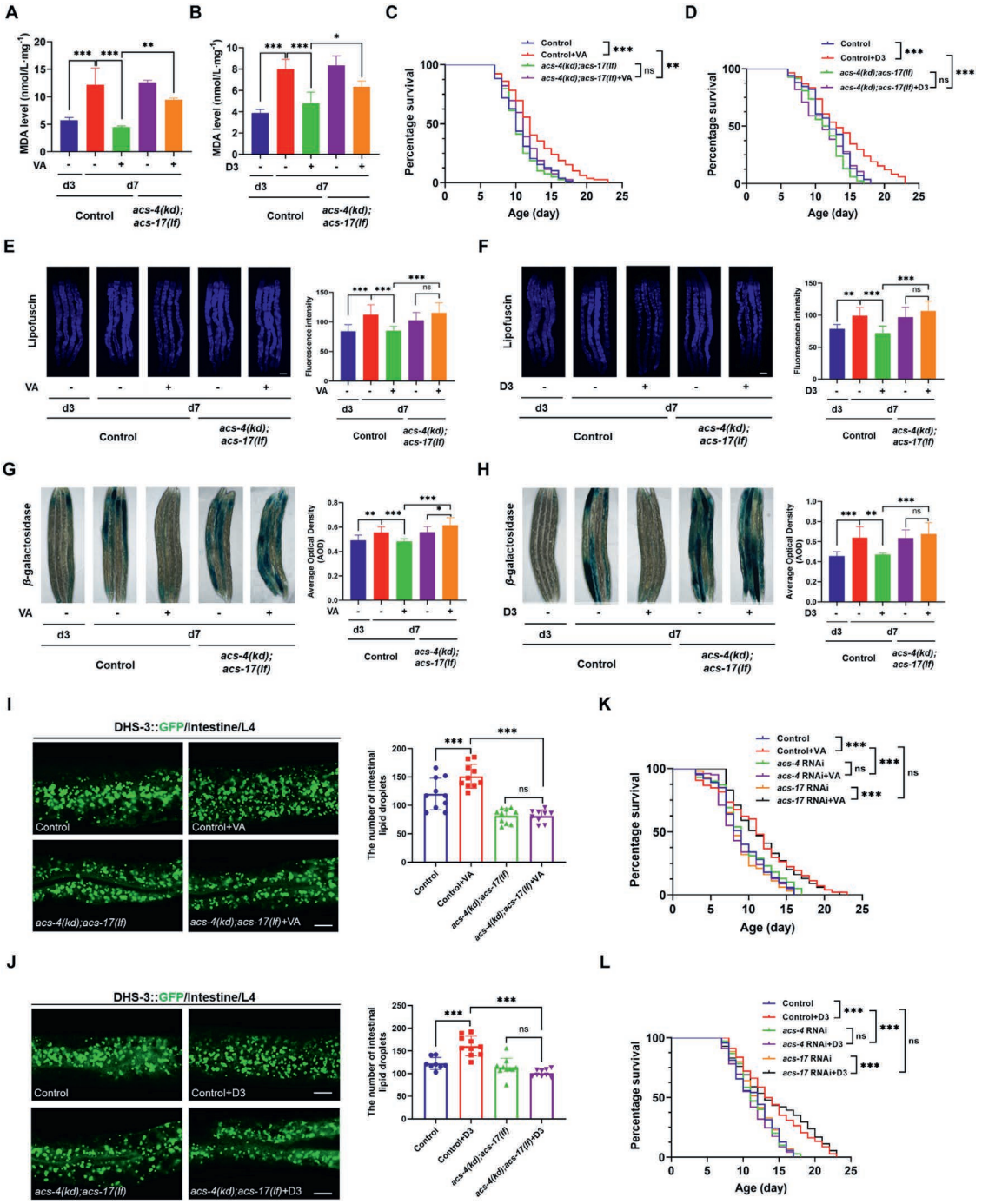

Figure 7 VA and its analogues D3 extend the lifespan of *C. elegans* in an ACSL3-dependent manner. (A, B) Relative MDA levels during aging and following supplementation with VA (A) and D3 (B) in *acs-4(kd)*;*acs-17(lf)* worms. "d" indicates days. (C, D) Survival analysis in control and *acs-4(kd)*;*acs-17(lf)* worm supplementation with VA (C) or D3 (D). Survival curves were represented the mean ± SEM and analyzed by log-rank test ($n \geq 60$ for each curve). (E, F) Representative autofluorescence images and quantification of the intestinal lipofuscin accumulation in control and *acs-4(kd)*;*acs-17(lf)* worms treated with VA (E) or D3 (F) on Days 3 and 7 of adulthood. scale bars: 100 μm, $n \geq 12$ worms per group. (G, H) Representative bright-field images and quantification of the average optical density of whole worms showed senescence-associated β-galactosidase (SA-β-GAL) staining (blue) on Day 3 and 7 in control and *acs-4(kd)*;*acs-17(lf)* worms treated with VA (G) or D3(H), scale bars: 100 μm, $n \geq 13$ worms per group. (I, J) Number of intestinal lipid droplets assessed by fluorescence, in *dhs-3p*:*dhs-3*:*GFP* worms with *acs-4(kd)*;*acs-17(lf)* group following VA (I) and D3 (J) supplementation, respectively. Fluorescence images of the intestine (left). Scale bars, 10 μm. Quantitative analysis of lipid droplets (right), $n = 10$ for each group. (K, L) Survival analysis in control, *acs-4(kd)*;*acs-17(lf)* worm supplementation with VA (K) or D3 (L). Survival curves were represented the mean ± SEM and analyzed by log-rank test ($n \geq 60$ for each curve). Data shown represent the mean ± SD. $^*P < 0.05$, $^{**}P < 0.01$, and $^{***}P < 0.001$ compared with the group treated with vehicle. ns means no significance.

proliferation of mutant *KRAS*-driven lung cancer cells[56]. Its knockout reduces tumor fibrosis and suppresses PDAC (pancreatic ductal adenocarcinoma) progression[57]. A recent study further demonstrated that radioresistant colorectal and lung tumors rely on ACSL3-meidated MUFA metabolic reprogramming to evade ferroptosis, and combining ACSL3 inhibition with ferroptosis inducers restored radiosensitivity in these treatment-resistant malignancies[58]. While ATRA has been established as a standard treatment for acute promyelocytic leukemia (APL), clinical trials have not demonstrated equivalent efficacy of ATRA in solid tumors, attributing this discrepancy to the development of resistance to ATRA[59]. Though the precise mechanism underlying ATRA resistance in solid tumors is not yet fully understood, our findings point to a potential link between high ACSL3 expression and drug resistance in these cancers, which warrants further investigations. Furthermore, our study demonstrated that VA analogues treatment notably reduced the inflammatory response and improved the pathogenesis of ConA-induced ALI and hepatic I/R injury[37,60]. Given that VA and ATRA have well-established pharmacokinetic profiles as clinical drugs[61,62], they exhibit substantial potential for application in the treatment of ferroptosis-related diseases.

Intriguingly, we demonstrate that VA analogues extend *C. elegans* lifespan in an ACSL3-dependent manner. Accumulation of MUFAs have recently been found to decrease lipid oxidation through upregulation of the MUFA/PUFA-PLs ratio during aging, which is beneficial to longevity[26]. Another study reported that VA extends lifespan and reduces lipofuscin and fat accumulation in *C. elegans via* transcriptionally upregulating SKN-1/NRF2[63]. Consistent with these findings, we confirm that VA extends lifespan by mitigating lipid peroxidation. Moreover, the observation that compound D3 exerts a similar effect underscores that VA analogues prolong lifespan through a distinct mechanism dependent on ACSL3-mediated MUFAs metabolism. Notably, this effect is specifically mediated by *acs-4*- not its paralogue *acs-17*-despite both being orthologues of human *ACSL3*. This suggests that *acs-4* and *acs-17* may function differentially in *C. elegans*, which warrants further investigation.

Translating *C. elegans* lifespan findings to mammals involves complexities stemming from biological distinctions. Mammalian lipid metabolism, for instance, is more intricate, featuring specialized cell types and complex transport mechanisms, compared to the simpler lipid storage in nematodes. These variations could influence how VA and its analogues affect mammalian lipid profiles and cellular responses, potentially leading to different longevity outcomes. Furthermore, while homologous, *C. elegans* Acs-4 and Acs-17 may exhibit functional nuances compared to the multifaceted human ACSL family. Thus, targeting ACSL3 in *C. elegans* might have distinct or more complex effects in mammals. This underscores the need for future mammalian studies to validate and precisely define the therapeutic potential of VA analogues in human aging and ferroptosis-related conditions.

4. Conclusions

In conclusion, our work uncovers a novel biological activity of VA and its analogues in MUFAs metabolism, which offers a novel strategy for the treatment of ferroptosis-related diseases and prolonging longevity.

5. Experimental

5.1. Chemicals and reagents

Vitamin A (S5592) and ATRA (S1653) were purchased from Selleck (Shanghai, China). All-*trans*-retinal (T5256), Fenretinide (T1872), Acitretin (T1330), AGN193109 (TQ0097), HX531 (T22843), Ch55 (T14946), Adapalene (T1093) and A939572 (T4515) were purchased from TargetMOI (Shanghai, China). BODIPY™ 581/591 C11 was obtained from Thermo. Staurosporine (HY-15141) was purchased from MedChemExpress (Shanghai, China). 2,2′-Azobis(2 methylpropionamidine) dihydrochloride (AAPH, 440914), 2,2-diphenyl-1-picrylhydrazyl (DPPH, D9132) and Egg-PC (840051P, Avanti Polar Lipids) were purchased from Sigma. Hieff Trans®Polyethylenimine Linear (PEI, 40816) was purchased from YESEN (Shanghai, China). PolyJet™ (SL100688) was purchased from SignaGen Laboratories.

5.2. General chemistry for the synthesis of VA analogues

All starting materials and reagents were either obtained from commercial suppliers or prepared according to procedures reported in the literature. All purchased chemicals and solvents were used without further purification unless otherwise noted. Flash chromatography was performed using silica gel (200−300 mesh or 300−400 mesh). All reactions were monitored by thin-layer chromatography (TLC) on silica gel plates with fluorescence indicator F254, which were visualized under UV light. NMR spectra were recorded on a Bruker AVANCE III 600 instrument, using CDC_{13} or DMSO-d_6 as solvents. All reagents were sourced from commercial suppliers (Sigma−Aldrich, Adamas, J&K, Innochem, TCI, and Acros) and used without further purification. The general procedures for synthesizing the VA analogues, along with the corresponding characterization data, are included in the supporting information.

5.3. Cell culture

HT-1080, 786-O, 769-P, SK-HEP-1, HEK293T cell lines were acquired from American type culture collection (ATCC). ARPE-19 cell line was purchased from the Cell Banks of Type Culture Collection of the Chinese Academy of Sciences. All cells were grown in Dulbecco's modified Eagle's medium supplemented with 10% fetal bovine serum (ExCell Bio), 100 U/mL of penicillin and 100 μg/mL of streptomycin in a 37 °C incubator with 5% CO_2 humidified atmosphere. ARPE-19 cells were cultured with DMEM/F12 medium. HT-1080 GPX4 KO cells were grown in DMEM medium supplemented with 1 μmol/L of Fer-1.

5.4. Cell viability assay

Cells were seeded on 96-well plates (10,000 cells per well) and treated with RSL3 or Erastin in the presence or absence of the indicated compounds for 24 h. Cell viability was assessed using Cell-Titer Glo Luminescent Cell Viability Assay Kit (Beyotime Biotechnology, C0057S) according to the manufacturer's recommendations by a microplate reader.

5.5. Free radical-trapping capacity measurement

The DPPH and ABTS assays are widely used methods for the assessment of the antioxidant capacities of natural products, they both are spectrophotometric techniques based on quenching of stable radicals (ABTS or DPPH).

5.5.1. DPPH assay

The stable radical 2,2-diphenyl-1-picrylhydrazyl (DPPH) was dissolved in methanol to a final concentration of 50 μmol/L 1 mL of DPPH solution was added to 1 μL of each test compound dissolved in DMSO. Samples were inverted several times and incubated at room temperature for 30 min. The absorbance at 517 nm was recorded *via* a microplate reader and normalized to background (methanol only).

5.5.2. ABTS assay

Total Antioxidant Capacity Assay Kit with ABTS kit was purchased from Beyotime Biotechnology (S0119). 2,2′-Azino-bis (3-ethylbenzothiazoline-6-sulfonic acid) (ABTS) was used as a chromogenic reagent. All procedures were according to the manufacturer's recommendations by a microplate reader at 405 nm. ABTS assay measures the relative ability of antioxidants to scavenge the ABTS generated in aqueous phase, as compared with a Trolox standard.

5.6. Fluorescence-enabled inhibited autoxidation (FENIX) assay

A lipophilic radical initiator 2,2′-azobis (2-methylpropionamidine) dihydrochloride (AAPH) was used to generate lipid peroxyl radicals, while lipid peroxidation probe C11 BODIPY$^{581/591}$ was implemented to monitor the autoxidation reaction. Briefly, the prepared EggPC liposomes (1 mmol/L) and C11 BODIPY 581/591 (1 μmol/L) in PBS were added to a black 96-well plate. The plate was incubated for 5 min at room temperature. This was followed by addition of VA, retinal, ATRA, C4, C5, D2, D3 and Fer-1 in different concentrations. Then the autoxidation was initiated by the addition of AAPH (1 mmol/L) and mixing in a plate reader. The lipid peroxidation signals were acquired by excitation at 488 nm and emission was measured at 518 nm lasting for 3 h by a fluorescence microplate.

5.7. Measurement of cellular lipid peroxidation

HT-1080 cells were seeded into six-well plates. Cells were treated with RSL3 or Erastin in the presence or absence of the indicated compounds. After treatment, cells were stained with C11-BODIPY (581/591) (D3861; Thermo Fisher Scientific) for 30 min at 37 °C and then harvested by trypsinization. Cells were washed and resuspended in PBS, and then analyzed by a flow cytometer (Accuri C6; BD Biosciences). A minimum of 10,000 cells were analyzed per condition. Data analysis was performed using FlowJo_V10 software.

5.8. Cellular GSH level

HT-1080 cells were seeded into six-well plates. Cells were treated with RSL3 or Erastin in the presence or absence of Vitamin A and ATRA. Cells were collected, resuspended with protein removal reagent M and lysed through freezing and thawing. Total GSH levels were detected by GSH Assay Kit (Beyotime Biotechnology, S0053) following the manufacturer's protocol. Protein quantification was performed using the BCA assay kit.

5.9. Cellular ferric ion level

HT-1080 cells were seeded into black 96-well plates (10,000 cells per well). Cells were treated with Vitamin A, Retinal and ATRA for 4 h. DFO was used for a positive control. Cells were washed three times with PBS after treatment. Next cells were stained with 1 μmol/L of FerroOrange (Dojingo, F374) in PBS with indicated compounds for exactly 30 min at 37 °C and 5% CO_2. The fluorescence was measured at *E*x 543 nm/Em 580 nm *via* a microplate. Cell viability was detected for normalization.

5.10. RARE luciferase assay

The plasmid of pGL3-RARE-luciferase was from T. Michael Underhill (Addgene plasmid # 13458; http://n2t.net/addgene:13458;/RRID:/Addgene_13458). HEK293T cells were seeded in white 96-well plate. pGL3-RARE-luciferase plasmid at dose of 50 ng per well was transfected into cells with the PolyJet™ reagent (SignaGen). After transfection for 24 h, cells were treated with ATRA and its analogues in the presence or absence of pan RAR antagonist AGN193109 for another 24 h. The activation of RARE luciferase was detected with Lite Luciferase Reporter Assay Kit (Vazyme, DD1205). Cell viability was measured with Cell-Titer Glo assay for normalization.

5.11. Lip-MS analysis

HT-1080 cells were grown until approximately 80%−85% confluence, washed with ice-cold PBS, and lysed with PBS. After centrifuge for 10 min at 18,000×*g* at 4 °C, the supernatant was transferred to a new 1.5-mL tube. Protein concentration was measured with bicinchoninic acid (BCA) assay. A total of 100 μg protein per sample was used in next experiments. Cell lysate was incubated with DMSO or VA for 30 min at room temperature with shaking with a thermomixer, followed by digestion with protease K. The samples were separated on SDS-PAGE. The gel bands corresponding to the protected proteins were collected and analyzed *via* quantitative mass spectrometry using standard protein identification approaches. Lip-MS and data analysis were performed by Shanghai Applied Protein Technology Co., Ltd. According to the principle of Lip-MS, an increase in the abundance of the long peptide of a sequence and a decrease in the abundance of the corresponding short peptide are detected simultaneously, which may be a target sequence of compounds binding, named feature sequence.

5.12. Pull-down assay

Pull-down experiments were carried out to confirm the interaction between VA analogues and ACSL3. HT-1080 cells were grown until 90% confluence and lysed with RIPA lysis buffer containing protease inhibitors. Cell lysates were treated with probe D5 (5 μmol/L) in the presence or absence of D3 (50 μmol/L) and incubated for 2 h at 4 °C. A freshly premixed click chemistry cocktail (100 μmol/L Biotin-N3 from 100 mmol/L stock solution in DMSO, 100 μmol/L TBTA from 100 mmol/L freshly prepared stock solution in DMSO, 1 mmol/L TCEP from 1 mol/L freshly prepared stock solution in deionized water, and 1 mmol/L $CuSO_4$ from 1 mol/L freshly prepared stock solution in deionized water)

was added to the lysates, followed by UV irradiation (365 nm) for 30 min on ice. The reaction was further incubated for 2 h prior to precipitation with prechilled acetone at −20 °C. The proteins were collected by centrifugation (16,000×*g*, 10 min at 4 °C) and dissolved in PBS containing 1% SDS. Biotin-labeled proteins were collected by incubation with streptavidin beads (Cytiva) for 2 h at room temperature, the beads were washed with 1% SDS in PBS (thrice), 0.1% SDS in PBS (thrice), and PBS (thrice). The beads were boiled in Laemmli sample buffer followed by SDS-PAGE analysis.

5.13. CRISPR-Cas9-mediated gene knockout

sgRNAs targeting human *ACSL3*, *SCD1*, *RXRA*, *RXRB*, *PRDX6* and *TXNRD1* were cloned into the lentiviral lentiCRISPR_V2 vector. Lentiviral particles were generated by co-transfection into HEK293T cells with psPAX2 and pMD2.G packaging plasmids. Target cells were infected with lentivirus with addition of 8 μg/mL polybrene and selected with puromycin (1 μg/mL) or blasticidin (10 μg/mL). Single cells were sorted into 96-well plates and grown for 2−3 weeks. Each colony was examined by Western blot and genomic DNA PCR to confirm the deletion of target gene.

The sequences of sgRNAs used in this study are listed below:

sg*RXRA*: GCACATCTGCGCCATCTGCG, AAGCACATCTG CGCCATCTG

sg*RXRB*: TACGGGGTTTACAGCTGTGA, GGACAACAA AGACTGCACAG

sg*ACSL3*: AGCTATCATCCACTCGGCCC, CGAGTGGA TGATAGCTGCAC

sg*SCD1*: CAATGATCAGAAAGAGCCGT, GCCACCGCTCT TACAAAGCT

sg*PRDX6*: ATCCTCTACCCAGCTACCAC, GAAACGGATG CGGCCGACGG

sg*TXNRD1*: CCGTGCTGGTGAATCCTGCT, CCAGGGAT GCCCAAGTAACG.

5.14. Generation of overexpression stable cell lines

Human *ACSL3* gene and its mutant were cloned into a pLVX vector. HEK293T cells were transfected with either pLVX-empty vector, pLVX-*ACSL3* or pLVX-$ACSL3^{S288A}$, together with psPAX.2 and pMD2.G packaging plasmids. Target cells were infected with lentivirus with addition of 8 μg/mL polybrene. Stable cells were selected with blasticidin and protein expression was verified by Western blot.

5.15. Protein extraction and Western blot analysis

Cells were washed with PBS and lysed in RIPA buffer with protease inhibitor Cocktail (Selleck). After centrifugation, the supernatant was collected and mixed with 4x Laemmli sample buffer. Samples were separated on SDS-PAGE gels and analyzed by Western blot. Primary antibodies used were as follows: ACSL3 (Santa Cruz, sc-166374), ACSL3 (Proteintech, 20710-1-AP), ACSL4 (Proteintech, 66617-1-Ig), SLC7A11 (CST, 12691S), GPX4 (HuaBio, ER1803-15), IRP1 (CST, 20272S), TFRC (CST, 13113S), FTH1 (CST, 4393S), RXRA/RXRB (CST, 8589), SCD1 (Proteintech, 28678-1-AP), FSP1 (Proteintech, 20886-1-AP), HSP90 (Proteintech, 13171-1-AP), β-actin (Proteintech, 81115-1-RR) and Vinculin (Sigma, V9131). The secondary antibodies were anti-rabbit/mouse IgG (Jackson ImmunoResearch).

5.16. Real-time quantitative PCR (qRT-PCR)

RNA Purification Kit (EZBioscience) was used to isolate RNA from cells and tissues. Totally 1 μg of mRNA was used for cDNA synthesis with Reverse Transcription Mix II (with gDNA Remover, EZBioscience). qPCR was performed on a LightCycler480 Real-Time PCR machine (Roche). Gene expression levels were normalized to GAPDH. The primer sequences are listed as follow, *ACSL3*-F: TTCTGCTGTCCTGTTGGTC (human) *GAPDH*-F: GGAGCGAGATCCCTCCAAAAT (human); *Ptgs2*-F: TGCACTATGGTTACAAAAGCTGG (mouse), *Tnfα*-F: GGTGCCTATGTCTCAGCCTCTT (mouse) and *Gapdh*-F: AGGTCGGTGTGAACGGATTTG (mouse).

5.17. Targeted lipidomics

HT-1080 cells were treated with VA (5 μmol/L) and D3 (5 μmol/L) for 12 h, then cells were digested and counted. Cell precipitation was collected by centrifugation and used for Targeted lipidomics analysis. Lipidomic analysis was performed by LipidALL Technologies (Changzhou, China).

5.18. ACSL3 protein purification

Human *ACSL3* was subcloned into a pET28a-his-sumo vector and transduced into *E. coli* BL21 cells (DE3). Expression of fusion protein was induced with 0.5 mmol/L of isopropyl β-D-thiogalactopyranoside (IPTG) at 16 °C for 20 h. Bacteria cells were then pelleted, resuspended in lysis buffer (50 mmol/L Tris-HCl pH 7.4, 500 mmol/L NaCl, 1 mmol/L PMSF, 2 mmol/L DTT, 2 mmol/L $MgCl_2$, 1% DDM), and sonicated. ACSL3 fusion protein was purified by using Ni-NTA resin (Smart-Lifesciences, China) and a Superdex 200 column according to manufacturer's instructions.

5.19. Microscale thermophoresis (MST)

The MST measurement for the binding of VA analogues to ACSL3 was performed using Monolith NT.115 (NanoTemper). In brief, his-ACSL3 protein was stained with RED-tris-NTA (MO-L018, NanoTemper). A titration series of VA analogues concentrations was prepared, and equal volumes of labeled ACSL3 protein solution and VA analogues concentrations were mixed and incubated to achieve binding equilibrium. After incubation for 30 min at room temperature, all the samples were loaded into MST NT.115 standard glass capillaries and measurement was carried out, the binding affinity (K_d) was analyzed using the MO. affinity software.

5.20. ACSL3 enzyme activity

ACSL3 activity was measured as previously described[56]. Briefly, recombinant ACSL3 protein was incubated with VA, ATRA or D3 for 2 h at 37 °C in a 200-μL reaction system containing 100 mmol/L Tris (pH 7.4), 5 mmol/L DTT, 5 mmol/L $MgCl_2$, 10 mmol/L ATP, 200 μmol/L CoA, 50 μmol/L OA and 0.03% Triton X-100. The reaction was terminated by adding 400 μL of acetonitrile and full vortex to extract. Centrifugation was performed at 13,000×*g* for 10 min, and the upper liquid was collected to be dried in the SpeedVac Vacuum Concentrator. Next, 100 μL methyl alcohol was added to fully dissolve the sample. Then, the samples were centrifuged at 13,000×*g* for 10 min, and the upper liquid was taken for LC−MS detection. OA-CoA was analyzed by LC−MS using an Ultimate-Orbitrap Exploris120 system using a Hypersil GOLD™ C_{18}

column (1.9 μm, 100 mm × 2.1 mm). Mobile phase A consists of methyl alcohol with 0.05% ammonia, and mobile phase B consists of water with 0.05% ammonia. The gradient elution program was set as follows: 0−0.5 min, 98% B; 0.5−4 min, 55% B; 4−6.5 min, 10% B; 6.5−9 min, 2% B; 9−10 min, 98% B. A 2 μL aliquot of each sample was injected for analysis.

5.21. Molecular docking of VA analogues with ACSL3

To elucidate the binding modes of VA analogues with their target, ACSL3, a protein structure-based molecular docking study was conducted utilizing the predicted structure of ACSL3 derived from AlphaFold 2. PrankWeb was employed to identify binding pockets for the docking analysis, successfully generating twelve binding sites under default parameters. Following this, compounds VA, ATRA, and D3 were docked into the predicted binding site using AutoDock Vina, as facilitated by PrankWeb.cz. The three-dimensional structures of the ligands were generated using the RDKit cheminformatics package and optimized using the Merck Molecular Force Field (MMFF) with a maximum number of iterations set to 20,000. The protein structure and the optimized ligand structure were prepared using two Python scripts, "prepare_receptor.py" and "prepare_ligand.py", respectively, with all preparation parameters set to default. The molecular docking engine used was Autodock Vina 1.2.3, with the scoring function set to "vina", and other key parameters set to "exhaustiveness = 16", "energy_range = 3".

5.22. ConA-induced acute immune hepatitis (AIH)

Male C57BL/6 mice (4−6 weeks) were purchased from GemPharmatech (Jiangsu, China) and bred in SPF-class housing of laboratory. All the animal experiments were approved by the National Institutional Animal Care and Ethical Committee of Chongqing Medical University (IACUC-CQMU-2024-09053). Animal suffering was minimized according to the Guidelines of the National Institutes of Health for the Care and Use of Laboratory Animals. ConA (Sigma, L7647) was dissolved in pyrogen-free normal saline solution to induce hepatitis by intravenous administration at a dose of 15 mg/kg. Mice were pretreated intraperitoneally with low and high dosage of VA (10 and 30 mg/kg), ATRA (10 and 30 mg/kg), D3 (10 and 30 mg/kg) and Fer-1 (5 mg/kg) for 24 h, followed by an additional treatment for 0.5 h before the injection of ConA. These compounds were dissolved in 5% DMSO and 95% Corn oil. After ConA administration for 24 h, mice were euthanized for blood collection. Serum AST and ALT levels were measured by an automatic biochemical analyzer. The liver tissues were collected and fixed for paraffin sections, and others were frozen quickly in liquid nitrogen for further research.

5.23. Hepatic ischemia/reperfusion (I/R) injury

Male C57BL/6 mice (8−10 weeks old) were used to produce the hepatic ischemia/reperfusion (I/R) injury model. Briefly, mice were pretreated intraperitoneally with VA (15 mg/kg) and D3 (15 mg/kg) for 48 and 24 h, followed by an additional treatment for 1 h before the operation. Mice were anesthetized with sodium pentobarbital. After opening the abdominal cavity, an atraumatic clip was placed across the portal vein, hepatic artery, and bile duct to interrupt blood supply to the left lateral and median lobes of the liver. After 60 min of ischemia, the clamp was removed and the liver was then reperfused. Mice were sacrificed 6 h after reperfusion, and samples of blood and ischemic lobes were collected.

5.24. Hematoxylin and eosin (H&E) staining and Immunohistochemistry (IHC)

Liver tissues were fixed in 4% paraformaldehyde and embedded with paraffin. Liver sections were deparaffinized and dehydrated by the usage of xylene and ethanol. For H&E staining, the sections were stained by hematoxylin and eosin, and sealed by using coverslip. For IHC, the specimens were blocked with 5% goat serum for 1 h at room temperature, and incubated at 4 °C overnight with 4-HNE antibody (Abcam, ab46545, 1: 200). Then, the liver slices were washed with PBS and incubated with secondary antibody for 1 h at 37 °C. DAB reagent was used for color development and hematoxylin was used for nuclear staining. The stained sections were sealed with neutral resin and analyzed by using a microscope (Olympus, Japan).

5.25. C. elegans strains, maintenance and treatment

Caenorhabditis elegans (*C. elegans*) were maintained on nematode growth medium (NGM) plates seeded with *E. coli* OP50. The following strains/alleles were obtained from the Caenorhabditis Genetics Center (CGC) or as indicated: N2 Bristol (wild-type strain), *acs-17(ok1562)*, *glp-4(bn2)*, *ldrIs1*[*dhs-3*p:*dhs-3*:GFP + *unc-76*(+)]. All experiments on *C. elegans* were supplemented with 17.5 mmol/L VA or its analogues D3, which was resuspended in water (with the assistance of ultrasound), or D3, which was dissolved in 2% DMSO (with the assistance of ultrasound). Prior to OP50 introduction, VA or D3 was applied to the surface of the NGM plates (100 μL per 6-cm dish) after the plates had fully cooled to room temperature following autoclaving. All resuspension procedures and experimental handling of VA or D3 were conducted in darkness to prevent photodegradation.

5.26. RNA interference

RNAi bacterial strains containing targeting genes were obtained from the Dharmacon RNAi collection, Cat#: RCE1181. Briefly, *E. coli* strain HT115(DE3) expressing dsRNA corresponding to each worm gene was grown overnight in LB broth containing 100 μg/mL ampicillin at 37 °C, then spread onto NGM plates containing 100 μg/mL ampicillin and 1 mmol/L IPTG. The RNAi-expressing bacteria were then grown overnight at 25 °C. Synchronized L4 larvae were placed on the seeded RNAi plates at 20 °C until animals reached maturity. Young adult worms were used for further experiments.

5.27. Lifespan assays

All lifespan assays were carried out at 25 °C, unless stated otherwise. The worms were synchronized using the bleaching method as previously described. Synchronized eggs were allowed to grow on NGM plates at 15 °C until they reached the early L4 stage, at which point they were shifted to 25 °C. The following day, young-adult worms were cultured on plates coated with VA or D3 and freshly cultured RNAi bacteria overnight. The adults were transferred to new petri dishes every two days until all the worms died.

5.28. Confocal microscopy for lipid droplets quantification

A reporter strain expressing the lipid droplet protein DHS-3 fused to GFP was used as a marker of lipid droplets in *C. elegans*. For each experiment, approximately 10 worms were imaged per condition. Synchronized L4 worms were imaged using laser scanning confocal microscopy (LSM 980, Carl Zeiss). The numbers of lipid droplets were analyzed in ImageJ software by applying the same threshold to all images and manually counting the lipid droplets in the same area.

5.29. MDA levels

The colorimetric reaction of malondialdehyde and thiobarbituric acid was used to detect malondialdehyde (MDA) content in mice liver and *C. elegans*. For liver in mice, about 100 mg of liver was lysed with MDA lysis buffer through a tissue grinder, then centrifuged at 22,000×*g* at 4 °C for 10 min, and supernatant was collected for analysis. For *C. elegans*, *glp-4(bn2)* and *glp-4(bn2)*; *acs-17(lf)* hermaphrodites were treated with control or *acs-4* RNAi, along with VA or D3 treatment for 3 or 7 days at 25 °C. Worms samples were ultrasonic treated (200 W, 3 s on, 10 s off, repeated 30 times), then centrifuged at 22,000×*g* at 4 °C for 10 min, and supernatant was collected for analysis. BCA Protein Assay Kit (Beyotime, P0010S) was used to determine the protein concentration. MDA levels were measured according to manufacturer's instructions (Solarbio, BC0025).

5.30. DAB-enhanced Prussian blue staining

DAB-enhanced Prussian blue was used for histochemical determination of iron storage in liver tissue. According to the protocol, the liver sections were placed into Prussian blue solution and incubated for 30 min at room temperature. DAB reagent was used for color development and hematoxylin was used for nuclear staining. All sections were then rinsed, dehydrated, cover-slipped, and digitized *via* light microscopy (Olympus, Japan).

5.31. Measurement of lipofuscin accumulation

To measure the accumulation of lipofuscin, synchronized hermaphrodites at L4 stage were treated with either control or *acs-4* RNAi, along with supplementation of either VA or D3. Worms were maintained at 25 °C for 3 or 7 days. After the treatment period, worms were immobilized on 2% (*w*/*v*) agarose pads for microscopy. Fluorescent images were captured using a Nexcope 910 microscopy system (Ningbo, China) (excitation/emission 360/460 nm). Lipofuscin levels were quantified by measuring the average fluorescence intensity across the entire body of each worm using ImageJ software (NIH).

5.32. Senescence-associated β-galactosidase activity assay

To measure senescence-associated β-galactosidase (SA-β-gal) activity, synchronized adult worms were collected on Days 3 or 7. Worms were first fixed in 4% paraformaldehyde for 30 s at room temperature and then permeabilized through four freeze-thaw cycles in liquid nitrogen. After fixation, worms were washed with PBS (pH 6.0) containing 0.1% Tween-20 and incubated overnight at 37 °C in a staining solution prepared using the Senescence β-Galactosidase Staining Kit (#9860, Cell Signaling Technology). Following the incubation, worms were mounted on 2% agarose pads and imaged using bright-field microscopy at 10 × magnification. The area of SA-β-gal staining was quantified by measuring the average optical density of the worm body using ImageJ software.

5.33. Statistical analysis

The data in figure legends are presented as mean ± standard deviation (SD). Statistical analyses were performed by one-way ANOVA for normally distributed data and by Kruskal−Wallis one-way ANOVA on ranks for data that were not normally distributed. When analysis of variance was significant, the Tukey/Dunn post hoc testing of differences between groups was performed. Full lifespan assays were assessed using standard Kaplan−Meier log-rank survival tests. All statistical analyses were performed using Prism 8.0 GraphPad software. $P < 0.05$ was considered significant.

Acknowledgments

We thank Dr. Bin Liang (Yunnan University, China) for providing worm strains and Dr. Zhiyi Wei (Southern University of Science and Technology, China) for the help in ACSL3 protein purification. This work was supported by National Key Research and Development Project of China (Nos. 2024YFC2815903 and 2018YFA0800304 to Hai-Xin Yuan, and 2024YFC2815904 to Shenyou Nie), the Supporting Fund for Innovation and Entrepreneurship by Chongqing Returned Oversea Scholars (No. cx2022012 to Hai-Xin Yuan and No. X9991 to Shenyou Nie, China), National Natural Science Foundation of China (32170781 to Zhe Zhang), Direct to PhD Program of Chongqing Science and Technology Commission (sl202100000610 to Shenyou Nie, China), Science and Technology Research Program of Chongqing Education Commission (KJQN202300414 to Shenyou Nie, China), Natural Science Foundation of Shandong Province (ZR2021QC023, 2023HWYQ-014, tsqn202306056 and 2021JK032 to Zhe Zhang, China), and Program for Youth Innovation in Future Medicine, Chongqing Medical University (W0176 to Hai-Xin Yuan and W0045 to Shenyou Nie, China).

Author contributions

Nanxuan Luo: Conceptualization, Data curation, Formal analysis, Investigation, Methodology, Project administration, Visualization, Writing-original draft, Writing e review & editing. Yijie Xiao: Investigation, Methodology, Visualization, Writing-original draft. Yile Zhai: Investigation, Methodology, Visualization, Writing-original draft. Jie Li: Investigation, Methodology, Formal analysis. Lijie Lv: Investigation, Methodology. Houhua Yin: Methodology. Fang Lin: Investigation, Methodology. Biwen Wan: Investigation, Methodology. Ke Zhang: Methodology. Junchi Hu: Investigation, Methodology. Junyan Liu: Methodology. Yongjun Dang: Conceptualization, Methodology. Yi He: Methodology, Project administration, Visualization. Yahui Zhao: Investigation, Methodology. Zhe Zhang: Funding acquisition, Project administration, Software, Writing-review & editing. Shenyou Nie: Conceptualization, Formal analysis, Project administration, Funding acquisition, Writing-review & editing. Hai-Xin Yuan: Funding acquisition, Investigation, Methodology, Resources, Supervision, Writing-review & editing.

Conflicts of interest

The authors declare no conflicts of interest.

Appendix A. Supporting information

Supporting information to this article can be found online at https://doi.org/10.1016/j.apsb.2025.11.004.

References

1. Dixon SJ, Lemberg KM, Lamprecht MR, Skouta R, Zaitsev EM, Gleason CE, et al. Ferroptosis: an iron-dependent form of non-apoptotic cell death. *Cell* 2012;**149**:1060−72.
2. Kagan VE, Mao G, Qu F, Angeli JP, Doll S, Croix CS, et al. Oxidized arachidonic and adrenic PEs navigate cells to ferroptosis. *Nat Chem Biol* 2017;**13**:81−90.
3. Doll S, Proneth B, Tyurina YY, Panzilius E, Kobayashi S, Ingold I, et al. ACSL4 dictates ferroptosis sensitivity by shaping cellular lipid composition. *Nat Chem Biol* 2017;**13**:91−8.
4. Yang WS, SriRamaratnam R, Welsch ME, Shimada K, Skouta R, ViswanathanVS, et al. Regulation of ferroptotic cancer cell death by GPX4. *Cell* 2014;**156**:317−31.
5. Bersuker K, Hendricks JM, Li Z, Magtanong L, Ford B, Tang PH, et al. The CoQ oxidoreductase FSP1 acts parallel to GPX4 to inhibit ferroptosis. *Nature* 2019;**575**:688−92.
6. Doll S, Freitas FP, Shah R, Aldrovandi M, da Silva MC, Ingold I, et al. FSP1 is a glutathione-independent ferroptosis suppressor. *Nature* 2019;**575**:693−8.
7. Mao C, Liu X, Zhang Y, Lei G, Yan Y, Lee H, et al. DHODH-mediated ferroptosis defence is a targetable vulnerability in cancer. *Nature* 2021; **593**:586−90.
8. Kraft VAN, Bezjian CT, Pfeiffer S, Ringelstetter L, Muller C, Zandkarimi F, et al. GTP cyclohydrolase 1/tetrahydrobiopterin counteract ferroptosis through lipid remodeling. *ACS Cent Sci* 2020;**6**: 41−53.
9. Mishima E, Ito J, Wu Z, Nakamura T, Wahida A, Doll S, et al. A non-canonical vitamin K cycle is a potent ferroptosis suppressor. *Nature* 2022;**608**:778−83.
10. Li Y, Ran Q, Duan Q, Jin J, Wang Y, Yu L, et al. 7-Dehydrocholesterol dictates ferroptosis sensitivity. *Nature* 2024;**626**:411−8.
11. Freitas FP, Alborzinia H, Santos AF dos, Nepachalovich P, Pedrera L, Zilka O, et al. 7-Dehydrocholesterol is an endogenous suppressor of ferroptosis. *Nature* 2024;**626**:401−10.
12. Yang WS, Kim KJ, Gaschler MM, Patel M, Shchepinov MS, Stockwell BR. Peroxidation of polyunsaturated fatty acids by lipoxygenases drives ferroptosis. *Proc Natl Acad Sci U S A* 2016;**113**: E4966−75.
13. Qiu B, Zandkarimi F, Bezjian CT, Reznik E, Soni RK, Gu W, et al. Phospholipids with two polyunsaturated fatty acyl tails promote ferroptosis. *Cell* 2024;**187**:1177.
14. Li Z, Hu Y, Zheng H, Li M, Liu Y, Feng R, et al. LPCAT1-mediated membrane phospholipid remodelling promotes ferroptosis evasion and tumour growth. *Nat Cell Biol* 2024;**26**:811−24.
15. Magtanong L, Ko PJ, To M, Cao JY, Forcina GC, Tarangelo A, et al. Exogenous monounsaturated fatty acids promote a ferroptosis-resistant cell state. *Cell Chem Biol* 2019;**26**:420.
16. Liang D, Feng Y, Zandkarimi F, Wang H, Zhang Z, Kim J, et al. Ferroptosis surveillance independent of GPX4 and differentially regulated by sex hormones. *Cell* 2023;**186**:2748.
17. Ubellacker JM, Tasdogan A, Ramesh V, Shen B, Mitchell EC, Martin-Sandoval MS, et al. Lymph protects metastasizing melanoma cells from ferroptosis. *Nature* 2020;**585**:113−8.
18. Tesfay L, Paul BT, Konstorum A, Deng Z, Cox AO, Lee J, et al. Stearoyl-CoA desaturase 1 protects ovarian cancer cells from ferroptotic cell death. *Cancer Res* 2019;**79**:5355−66.
19. Mao X, Wang X, Jin M, Li Q, Jia J, Li M, et al. Critical involvement of lysyl oxidase in seizure-induced neuronal damage through ERK−Alox5-dependent ferroptosis and its therapeutic implications. *Acta Pharm Sin B* 2022;**12**:3513−28.
20. Stockwell BR. Ferroptosis turns 10: emerging mechanisms, physiological functions, and therapeutic applications. *Cell* 2022;**185**: 2401−21.
21. Tong J, Li D, Meng H, Sun D, Lan X, Ni M, et al. Targeting a novel inducible GPX4 alternative isoform to alleviate ferroptosis and treat metabolic-associated fatty liver disease. *Acta Pharm Sin B* 2022;**12**: 3650−66.
22. Brown AR, Hirschhorn T, Stockwell BR. Ferroptosis-disease perils and therapeutic promise. *Science* 2024;**386**:848−9.
23. Jenkins NL, James SA, Salim A, Sumardy F, Speed TP, Conrad M, et al. Changes in ferrous iron and glutathione promote ferroptosis and frailty in aging *Caenorhabditis elegans*. *eLife* 2020;**9**:e56580.
24. Nishizawa H, Matsumoto M, Yamanaka M, Irikura R, Nakajima K, Tada K, et al. BACH1 inhibits senescence, obesity, and short lifespan by ferroptotic FGF21 secretion. *Cell Rep* 2024;**43**:114403.
25. Ren H, Yin K, Lu X, Liu J, Li D, Liu Z, et al. Synergy between nanoplastics and benzo[*a*]pyrene promotes senescence by aggravating ferroptosis and impairing mitochondria integrity in *Caenorhabditis elegans*. *Sci Total Environ* 2024;**946**:174418.
26. Papsdorf K, Miklas JW, Hosseini A, Cabruja M, Morrow CS, Savini M, et al. Lipid droplets and peroxisomes are co-regulated to drive lifespan extension in response to mono-unsaturated fatty acids. *Nat Cell Biol* 2023;**25**:672−84.
27. Tschuck J, Padmanabhan Nair V, Galhoz A, Zaratiegui C, Tai HM, Ciceri G, et al. Suppression of ferroptosis by vitamin A or radical-trapping antioxidants is essential for neuronal development. *Nat Commun* 2024;**15**:7611.
28. Wang TX, Duan KL, Huang ZX, Xue ZA, Liang JY, Dang Y, et al. Tanshinone functions as a coenzyme that confers gain of function of NQO1 to suppress ferroptosis. *Life Sci Alliance* 2023;**6**:e202201667.
29. Penniston KL, Tanumihardjo SA. The acute and chronic toxic effects of vitamin A. *Am J Clin Nutr* 2006;**83**:191−201.
30. de Thé H, Vivanco-Ruiz MM, Tiollais P, Stunnenberg H, Dejean A. Identification of a retinoic acid responsive element in the retinoic acid receptor beta gene. *Nature* 1990;**343**:177−80.
31. Tierney MT, Polak L, Yang Y, Abdusselamoglu MD, Baek I, Stewart KS, et al. Vitamin A resolves lineage plasticity to orchestrate stem cell lineage choices. *Science* 2024;**383**:eadi7342.
32. Hashimoto Y, Kagechika H, Shudo K. Expression of retinoic acid receptor genes and the ligand-binding selectivity of retinoic acid receptors (RAR's). *Biochem Biophys Res Commun* 1990;**166**:1300−7.
33. Shroot B, Michel S. Pharmacology and chemistry of adapalene. *J Am Acad Dermatol* 1997;**36**:S96−103.
34. Bi G, Liang J, Shan G, Bian Y, Chen Z, Huang Y, et al. Retinol saturase mediates retinoid metabolism to impair a ferroptosis defense system in cancer cells. *Cancer Res* 2023;**83**:2387−404.
35. Osanai M. Cellular retinoic acid bioavailability in various pathologies and its therapeutic implication. *Pathol Int* 2017;**67**:281−91.
36. Zeng T, Deng G, Zhong W, Gao Z, Ma S, Mo C, et al. Indoleamine 2,3-dioxygenase 1enhanceshepatocytes ferroptosis in acute immune hepatitis associated with excess nitrative stress. *Free Radic Biol Med* 2020;**152**:668−79.
37. Yan B, Ai Y, Sun Q, Ma Y, Cao Y, Wang J, et al. Membrane damage during ferroptosis is caused by oxidation of phospholipids catalyzed by the oxidoreductases POR and CYB5R1. *Mol Cell* 2021; **81**:355.
38. Friedmann Angeli JP, Schneider M, Proneth B, Tyurina YY, Tyurin VA, Hammond VJ, et al. Inactivation of the ferroptosis regulator Gpx4 triggers acute renal failure in mice. *Nat Cell Biol* 2014;**16**: 1180−91.
39. Yamada N, Karasawa T, Wakiya T, Sadatomo A, Ito H, Kamata R, et al. Iron overload as a risk factor for hepatic ischemia−reperfusion injury in liver transplantation: potential role of ferroptosis. *Am J Transplant* 2020;**20**:1606−18.

40. Wang H, Klein MG, Zou H, Lane W, Snell G, Levin I, et al. Crystal structure of human stearoyl-coenzyme A desaturase in complex with substrate. *Nat Struct Mol Biol* 2015;**22**:581−5.
41. Vrablik TL, Petyuk VA, Larson EM, Smith RD, Watts JL. Lipidomic and proteomic analysis of *Caenorhabditis elegans* lipid droplets and identification of ACS-4 as a lipid droplet-associated protein. *Biochim Biophys Acta* 2015;**1851**:1337−45.
42. Kitisin T, Muangkaew W, Sukphopetch P. *Caenorhabditis elegans* DAF-16 regulates lifespan and immune responses to Cryptococcus neoformans and Cryptococcus gattii infections. *BMC Microbiol* 2022;**22**:162.
43. Venz R, Goyala A, Soto-Gamez A, Yenice T, Demaria M, Ewald CY. *In vivo* screening implicates endoribonuclease regnase-1 in modulating senescence-associated lysosomal changes. *Geroscience* 2024; **46**:1499−514.
44. Zhang P, Na H, Liu Z, Zhang S, Xue P, Chen Y, et al. Proteomic study and marker protein identification of *Caenorhabditis elegans* lipid droplets. *Mol Cell Proteomics* 2012;**11**:317−28.
45. Zeng L, Li X, Preusch CB, He GJ, Xu N, Cheung TH, et al. Nuclear receptors NHR-49 and NHR-79 promote peroxisome proliferation to compensate for aldehyde dehydrogenase deficiency in C. elegans. *PLoS Genet* 2021;**17**:e1009635.
46. Melis M, Tang XH, Trasino SE, Gudas LJ. Retinoids in the pathogenesis and treatment of liver diseases. *Nutrients* 2022;**14**:1456.
47. Cañón E, Cosgaya JM, Scsucova S, Aranda A. Rapid effects of retinoic acid on CREB and ERK phosphorylation in neuronal cells. *Mol Biol Cell* 2004;**15**:5583−92.
48. Gupta P, Ho PC, Huq MM, Ha SG, Park SW, Khan AA, et al. Retinoic acid-stimulated sequential phosphorylation, PML recruitment, and SUMOylation of nuclear receptor TR2 to suppress Oct4 expression. *Proc Natl Acad Sci U S A* 2008;**105**:11424−9.
49. Wei S, Kozono S, Kats L, Nechama M, Li W, Guarnerio J, et al. Active Pin1 is a key target of all-*trans* retinoic acid in acute promyelocytic leukemia and breast cancer. *Nat Med* 2015;**21**:457−66.
50. Xue JH, Chen GD, Hao F, Chen H, Fang Z, Chen FF, et al. A vitamin-C-derived DNA modification catalysed by an algal TET homologue. *Nature* 2019;**569**:581−5.
51. Kovatcheva M, Melendez E, Chondronasiou D, Pietrocola F, Bernad R, Caballe A, et al. Vitamin B12 is a limiting factor for induced cellular plasticity and tissue repair. *Nat Metab* 2023;**5**:1911−30.
52. Swamynathan MM, Kuang S, Watrud KE, Doherty MR, Gineste C, Mathew G, et al. Dietary pro-oxidant therapy by a vitamin K precursor targets PI 3-kinase VPS34 function. *Science* 2024;**386**: eadk9167.
53. Tesoriere L, Ciaccio M, Bongiorno A, Riccio A, Pintaudi AM, Livrea MA. Antioxidant activity of all-*trans*-retinol in homogeneous solution and in phosphatidylcholine liposomes. *Arch Biochem Biophys* 1993;**307**:217−23.
54. Keys SA, Zimmerman WF. Antioxidant activity of retinol, glutathione, and taurine in bovine photoreceptor cell membranes. *Exp Eye Res* 1999;**68**:693−702.
55. Blaner WS, Shmarakov IO, Traber MG. Vitamin A and Vitamin E: will the real antioxidant please stand up?. *Annu Rev Nutr* 2021;**41**: 105−31.
56. Padanad MS, Konstantinidou G, Venkateswaran N, Melegari M, Rindhe S, Mitsche M, et al. Fatty acid oxidation mediated by acyl-CoA synthetase long chain 3 is required for mutant *KRAS* lung tumorigenesis. *Cell Rep* 2016;**16**:1614−28.
57. Rossi Sebastiano M, Pozzato C, Saliakoura M, Yang Z, Peng RW, Galiè M, et al. ACSL3−PAI-1 signaling axis mediates tumor-stroma cross-talk promoting pancreatic cancer progression. *Sci Adv* 2020;**6**: eabb9200.
58. Cao Y, Li J, Chen Y, Wang Y, Liu Z, Huang L, et al. Monounsaturated fatty acids promote cancer radioresistance by inhibiting ferroptosis through ACSL3. *Cell Death Dis* 2025;**16**:184.
59. Costantini L, Molinari R, Farinon B, Merendino N. Retinoic acids in the treatment of most lethal solid cancers. *J Clin Med* 2020; **9**:360.
60. Friedmann Angeli JP, Schneider M, Proneth B, Tyurina YY, Tyurin VA, Hammond VJ, et al. Inactivation of the ferroptosis regulator Gpx4 triggers acute renal failure in mice. *Nat Cell Biol* 2014;**16**: 1180−91.
61. Adamson PC, Bailey J, Pluda J, Poplack DG, Bauza S, Murphy RF, et al. Pharmacokinetics of all-*trans*-retinoic acid administered on an intermittent schedule. *J Clin Oncol* 1995;**13**:1238−41.
62. Chen C, Mistry G, Jensen B, Heizmann P, Timm U, van Brummelen P, et al. Pharmacokinetics of retinoids in women after meal consumption or vitamin A supplementation. *J Clin Pharmacol* 1996;**36**: 799−808.
63. Sirakawin C, Lin D, Zhou Z, Wang X, Kelleher R, Huang S, et al. SKN-1/NRF2 upregulation by vitamin A is conserved from nematodes to mammals and is critical for lifespan extension in *Caenorhabditis elegans*. *Aging Cell* 2024;**23**:e14064.